Chapter 2
Binary Emission Processes

2.1 General Remarks

Most of nuclei decay by emitting a particle like proton, neutron, electron, positron or a composite cluster as deuteron, α-particle, Be, C, O, Mg, Ne, Si. Heavy nuclei can also fission into two fragments with comparable sizes. All these decays are called binary emission processes and they can be written as follows

$$P(J_i M_i) \rightarrow D_1(J_1 M_1) + D_2(J_2 M_2), \tag{2.1}$$

where $J_i M_i$ is the initial spin and its projection. We suppose that other quantum numbers, like parity, are also embedded into this notation. The final spins J_k, $k = 1, 2$ satisfy the triangle rule

$$|J_1 - J_2| \leq J_i \leq J_1 + J_2, \tag{2.2}$$

and the initial parity equals the product of fragment parities.

As we already pointed out, our presentation concerns the description of decay processes induced only by the strong interaction. An important feature of these decays is connected with the large Coulomb barrier preventing the two fragments from moving apart. In the phenomenological description, we suppose that this barrier is extended in the internal region, so that the dynamics of the two fragments is fully described by a potential, defined for all distances. Such interaction is shown for the proton emission in Fig. 2.1, where it is given the spherical part of the Woods–Saxon potential, describing proton emission from ^{131}Eu. The energy of the system (dot-dashed line) is smaller that the height of the barrier, but the two fragments can penetrate it, due to the very small, but different from zero, wave function outside the barrier. We will show below, that this property can be described in terms of the so-called penetrability.

The main difficulty that one encounters when studying decay processes, not only from an experimental point of view, but also theoretically, is the instability of the initial nucleus. One may expect that these decay processes cannot be considered stationary and one has to use the time-dependent Schrödinger equation

D. S. Delion, *Theory of Particle and Cluster Emission*, Lecture Notes in Physics, 819,
DOI: 10.1007/978-3-642-14406-6_2, © Springer-Verlag Berlin Heidelberg 2010

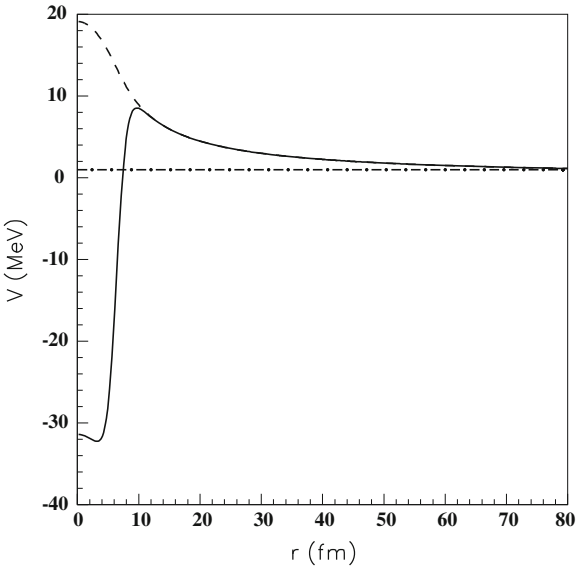

Fig. 2.1 Spherical part of the nuclear plus Coulomb interaction (*solid line*) as a function of the radius in ^{131}Eu. The Coulomb part (*dash line*) and the proton Q-value (*dot-dashed line*) are also shown

$$i\hbar\frac{\partial\Phi(t,\mathbf{r})}{\partial t} = \mathbf{H}\Phi(t,\mathbf{r}). \tag{2.3}$$

Anyway, due to large Coulomb barriers the probability of a cluster to escape from nucleus is very small and short lived states actually correspond to very narrow decay widths of such states, which are called resonant states. For instance, the shortest measurable half life is about $T_{1/2} = 10^{-12}$ s for proton emission, and the corresponding decay width is, according to the uncertainty relation

$$\Delta E\Delta t \sim \hbar, \tag{2.4}$$

$\Gamma \sim \Delta E = 6.6 \times 10^{-10}$ MeV. Since the characteristic nuclear time is $T_N \approx 10^{-22}$ s, the nucleus lives a long time before decaying in this energy-time scale and, therefore, the decay process may be considered stationary.

The wave function in the region of a resonance, with the width $\Delta E \sim \Gamma$, lying at an energy $E^{(0)}$ can be factorized in terms of the energy depending Lorentzian distribution as follows [1]

$$\begin{aligned}\Phi(E,\mathbf{r}) &= -\frac{\Gamma/2}{\pi\left[(E-E^{(0)})^2+(\Gamma/2)^2\right]}\Psi(\mathbf{r}) \\ &= \frac{1}{2\pi i}\left[\frac{1}{E-(E^{(0)}-i\Gamma/2)}-\frac{1}{E-(E^{(0)}+i\Gamma/2)}\right]\Psi(\mathbf{r}).\end{aligned} \tag{2.5}$$

The corresponding evolution in time is given by the Fourier transform, which can easily be estimated by using the Cauchy theorem

$$\Phi(t,\mathbf{r}) = \int_{-\infty}^{\infty} \Phi(E,\mathbf{r}) e^{-iEt/\hbar} dE = \Psi(\mathbf{r}) e^{-iE_r t/\hbar}, \tag{2.6}$$

and therefore it has the form of a stationary state, but with a complex energy

$$E_r = E^{(0)} - \frac{i}{2}\Gamma, \tag{2.7}$$

as first proposed by Gamow in his paper explaining α-decay as a quantum penetration process, thus imposing the probabilistic interpretation of the quantum mechanics [2]. In this way, a narrow resonant state behaves almost like a bound state. In the same year, a similar explanation was given by Condon and Gurwey in Ref. [3].

Gamow put forward this idea, novel for his time and bold even today, that since the time dependence of the wave function, corresponding to the decaying resonance, should have the stationary form (2.6), the resonance energy could be considered complex with the form (2.7).

This idea proved to be of great significance in the study of all resonant processes. One of its important consequences is that, by going to the complex energy plane, the theory becomes dubious and difficult, but it has the great feature of transforming a time dependent process into a stationary one [4].

2.2 Angular Momentum Representation

The general framework to describe emission processes is the stationary scattering theory. The main tool is the angular momentum representation of solutions. Firstly we will give a textbook version of the formalism for spherical nuclei emitting structureless fragments. Then we will generalize the formalism to deformed nuclei emitting fragments with a given structure.

2.2.1 Spherical Boson Emitters

Let us consider that the fragments are structureless bosons emitted from a spherical nucleus. The typical case is the α-decay, connecting ground states of even–even spherical nuclei. The stationary Schrödinger equation describing such a process is written as follows

$$\left[-\frac{\hbar^2}{2\mu}\Delta + V_0(r)\right]\Psi(\mathbf{r}) = E\Psi(\mathbf{r}), \tag{2.8}$$

where μ denotes the reduced mass of the α-daughter system. The potential, $V_0(r)$ between the α-particle and daughter nucleus has two components: the short range nuclear part $V_N(r)$ and the Coulomb interaction $V_C(r)$. The wave function can be expanded in partial waves in terms of spherical harmonics

$$\Psi(\mathbf{r}) = \sum_l \frac{f_l(r)}{r} Y_{lm}(\hat{r}), \tag{2.9}$$

where $\mathbf{r} = (r, \hat{r}) \equiv (r, \theta, \phi)$. The spherical harmonics are factorized as follows

$$Y_{ln}(\theta, \phi) = \Theta_{lm}(\theta)\Phi_m(\phi), \quad \Phi_m(\phi) = \frac{e^{im\phi}}{\sqrt{2\pi}}, \tag{2.10}$$

where each component is orthonormal

$$\begin{aligned} \int_0^\pi \Theta^*_{lm}(\theta)\Theta_{l'm'}(\theta)\sin\theta d\theta = \delta_{ll'} \\ \int_0^{2\pi} \Phi^*_m(\phi)\Phi_{m'}(\phi)d\phi = \delta_{mm'}. \end{aligned} \tag{2.11}$$

The Laplacian in spherical coordinates has the following form

$$\Delta = \frac{1}{r}\frac{\partial^2}{\partial r^2} r - \frac{\hat{L}^2}{r^2}, \tag{2.12}$$

where the angular part of the operator acts on spherical harmonics as follows

$$\hat{L}^2 Y_{lm}(\theta, \phi) = l(l+1)Y_{lm}(\theta, \phi). \tag{2.13}$$

We insert the expansion in partial waves (2.9) in (2.8) and then we multiply it with $Y^*_{lm}(\theta, \phi)$. By using the orthogonality of spherical harmonics (2.11), one obtains the following equations for radial components

$$\frac{d^2 f_l(r)}{dr^2} = \left\{ \frac{l(l+1)}{r^2} + \frac{2\mu}{\hbar^2}[V_0(r) - E] \right\} f_l(r). \tag{2.14}$$

This system of decoupled equations can also be written in terms of the dimensionless reduced radius $\rho = \kappa r$, depending on the momentum $\kappa = \sqrt{2\mu E}/\hbar$, as follows

$$\left[-\frac{d^2}{d\rho^2} + \frac{V_l(r)}{E} - 1 \right] f_l(r) = 0, \tag{2.15}$$

where we introduced the angular momentum-dependent potential,

$$\frac{V_l(r)}{E} = \frac{l(l+1)}{\rho^2} + \frac{V_0(r)}{E}. \tag{2.16}$$

Since the nuclear interaction V_N is of a finite range, one has $V_N(r) = 0$ beyond some radius. Therefore at large distances only the spherical Coulomb interaction is active and the ratio between the interaction potential and emission energy can be expressed as follows

$$\frac{V_0(r)}{E} \to \frac{Z_1 Z_2 e^2}{rE} = \frac{\chi}{\rho}, \tag{2.17}$$

where Z_k are the charges of emitted fragments. Here we introduced the Coulomb parameter (twice the Sommerfield parameter)

$$\chi = 2\frac{Z_1 Z_2 e^2}{\hbar v}, \tag{2.18}$$

with the asymptotic velocity defined as follows

$$v = \sqrt{\frac{2E}{\mu}} = \frac{\hbar\kappa}{\mu}. \tag{2.19}$$

The independent solutions of the Coulomb equation

$$\left[-\frac{d^2}{d\rho^2} + \frac{l(l+1)}{\rho^2} + \frac{\chi}{\rho} - 1\right] f_l(r) = 0, \tag{2.20}$$

are the standard regular and irregular Coulomb functions [5]. They are real functions of ρ. The regular solution $F_l(\chi, \rho)$ vanishes at the origin and increases as a function of the distance inside the Coulomb barrier, while the irregular solution $G_l(\chi, \rho)$ diverges at the origin but decreases with distance inside the Coulomb barrier.

At large distances both solutions oscillate, i.e. their asymptotic behaviour is given by

$$\begin{aligned} f_l(\chi,\rho) = F_l(\chi,\rho) &\to_{\rho\to\infty} \sin\left(\rho - \frac{1}{2}l\pi + \sigma_l\right), \\ G_l(\chi,\rho) &\to_{\rho\to\infty} \cos\left(\rho - \frac{1}{2}l\pi + \sigma_l\right). \end{aligned} \tag{2.21}$$

where σ_l is the Coulomb phase shift

$$\sigma_l = \arg\Gamma\left(l + 1 + i\frac{\chi}{2}\right) - \frac{1}{2}\chi \ln 2\rho, \tag{2.22}$$

with Γ being the Euler Gamma-function. In the above definition we also included the term depending upon the logarithm of the reduced radius.

If one of the emitted fragments is neutral, like for instance the neutron, then $\sigma_l = 0$ and the above spherical waves are proportional to spherical Bessel functions

$$\begin{aligned} f_l(\rho) &= \rho j_l(\rho) \rightarrow_{\rho\rightarrow\infty} \sin\left(\rho - \frac{1}{2}l\pi\right) \\ &= \rho n_l(\rho) \rightarrow_{\rho\rightarrow\infty} \cos\left(\rho - \frac{1}{2}l\pi\right). \end{aligned} \tag{2.23}$$

The outgoing/ingoing Coulomb–Hankel waves are defined in terms of the above Coulomb functions as follows

$$H_l^{(\pm)}(\chi,\rho) = G_l(\chi,\rho) \pm iF_l(\chi,\rho) \rightarrow_{\rho\rightarrow\infty} exp\left[\pm i\left(\rho - \frac{1}{2}l\pi + \sigma_l\right)\right]. \tag{2.24}$$

These waves become usual Hankel functions for neutral particles, i.e.

$$\rho h_l^{(\pm)}(\rho) = \rho[n_l(\rho) + ij_l(\rho)] \rightarrow_{\rho\rightarrow\infty} exp\left[\pm i\left(\rho - \frac{1}{2}l\pi\right)\right]. \tag{2.25}$$

2.2.2 Spherical Fermion Emitters

In the case of fermion (proton or neutron) emission from spherical nuclei the central potential entering Schrödinger equation (2.8) contains also the spin-orbit part, i.e.

$$V_0(r,\mathbf{s}) = V_0(r) + V_{so}(r)\mathbf{l}.\boldsymbol{\sigma}, \tag{2.26}$$

where $V_0(r)$ is the central nuclear plus Coulomb potential and $\boldsymbol{\sigma} = 2\mathbf{s}$. The wave function is expanded

$$\Psi(\mathbf{r},\mathbf{s}) = \sum_l \frac{f_{lj}(r)}{r} \mathscr{Y}_{jm}^{(l)}(\hat{r},\mathbf{s}), \tag{2.27}$$

in terms of spin-orbital harmonics

$$\mathscr{Y}_{jm}^{(l)}(\hat{r},\mathbf{s}) = \left[Y_l(\hat{r}) \otimes \chi_{\frac{1}{2}}(\mathbf{s})\right]_{jm} \equiv \sum_{m_1+m_2=m} \langle lm_1;\frac{1}{2}m_2|jm\rangle Y_{lm_1}(\hat{r})\chi_{\frac{1}{2}m_2}(\mathbf{s}), \tag{2.28}$$

where the bracket symbol denotes Clebsch–Gordan recoupling coefficients corresponding to the angular momentum addition $\mathbf{j} = \mathbf{l} + \mathbf{s}$. By using the same manipulations as in the previous case one obtains the system of equations for radial components

$$\left[-\frac{d^2}{d\rho^2}+\frac{l(l+1)}{\rho^2}+\frac{V_0(r)+V_{so}(r)\langle \mathbf{l}.\boldsymbol{\sigma}\rangle}{E}-1\right]f_{lj}=0, \tag{2.29}$$

where

$$\langle \mathbf{l}.\boldsymbol{\sigma}\rangle = j(j+1)-l(l+1)-\frac{3}{4}. \tag{2.30}$$

At large distances the system contains only Coulomb interaction (2.17).

2.3 S-Matrix

In this section we will investigate the so-called scattering states, i.e. real solutions of the Schrödinger equation with positive energy. The formalism presented below is common for boson and fermion cases. In order to simplify notations we will use boson channel notation l. For the fermion emission this index should be replaced by $l \rightarrow (lj)$.

2.3.1 Scattering States

In the external region, where the nuclear interaction vanishes, the solution is a combination of the Coulomb functions. The standard form that one adopts is the following

$$\begin{aligned} f_l^{(\mathrm{ext})}(E,r) &\sim G_l(\chi,\rho)\sin\delta_l(E)+F_l(\chi,\rho)\cos\delta_l(E) \\ &= \frac{i}{2}e^{-i\delta_l(E)}\left[H_l^{(-)}(\chi,\rho)-\mathscr{S}_l(E)H_l^{(+)}(\chi,\rho)\right]. \end{aligned} \tag{2.31}$$

Notice that this form is valid for spherical emitters, where in each spherical channel, corresponding to a given angular momentum l, there is an incoming wave $H_l^{(-)}$. Later on, in the Section devoted to the R-matrix method, we will give a more general expression corresponding to deformed emitters. We will show below that the phase shift is a real number, so that the S-matrix, defined by

$$\mathscr{S}_l(E)=e^{2i\delta_l(E)}, \tag{2.32}$$

satisfies the unitarity condition

$$\mathscr{S}_l(E)\mathscr{S}_l^{\dagger}(E)=1. \tag{2.33}$$

To evaluate the phase shift, and therefore the S-matrix, one requires the continuity of the external and internal wave functions and of the corresponding derivatives at the point $r = R$. The internal wave function should be regular in origin

$$f_l^{(\mathrm{int})}(r \to 0) \to r^{l+1}. \tag{2.34}$$

This is achieved through the matching of the internal and external logarithmic derivatives of the wave function $f_l(r)$, i.e.

$$\beta_l^{(\mathrm{int})}(R) \equiv \frac{1}{f_l^{(\mathrm{int})}(R)} \frac{df_l^{(\mathrm{int})}(R)}{dr} = \beta_l^{(\mathrm{ext})}(R) \equiv \frac{1}{f_l^{(\mathrm{ext})}(R)} \frac{df_l^{(\mathrm{ext})}(R)}{dr}. \tag{2.35}$$

From Eq. 2.31, writing the trigonometric functions in terms of exponentials, one gets

$$\mathscr{S}_l(E) = e^{2i\overline{\delta}_l(E,R)} \frac{\beta_l^{(int)}(E,R) - D_l(E,R) + iP_l(E,R)}{\beta_l^{(int)}(E,R) - D_l(E,R) - iP_l(E,R)}. \tag{2.36}$$

where we have defined

$$\begin{aligned}
D_l(E,R) &\equiv kR \frac{F_l'(\chi,\kappa R) + iG_l'(\chi,\kappa R)}{F_l^2(\chi,\kappa R) + G_l^2(\chi,\kappa R)} = i\kappa R \frac{\left[H_l^{(-)}(\chi,\kappa R)\right]'}{\left|H_l^{(+)}(\chi,\kappa R)\right|^2}, \\
P_l(E,R) &\equiv \frac{\kappa R}{F_l^2(\chi,\kappa R) + G_l^2(\chi,\kappa R)} = \frac{\kappa R}{\left|H_l^{(+)}(\chi,\kappa R)\right|^2}, \\
e^{2i\overline{\delta}_l(E,R)} &\equiv -\frac{F_l(\chi,\kappa R) + iG_l(\chi,\kappa R)}{F_l(\chi,\kappa R) - iG_l(\chi,\kappa R)} = \frac{H_l^{(-)}(\chi,\kappa R)}{H_l^{(+)}(\chi,\kappa R)},
\end{aligned} \tag{2.37}$$

with, e.g. $F_l'(\chi,\kappa R) \equiv dF_l(\chi,\rho)/d\rho|_{\rho=\kappa R}$. We have also used the property that the Wronskian for Coulomb functions is unity, i. e. $F_l'(\chi,\rho)G_l(\chi,\rho) - G_l'(\chi,\rho)F_l(\chi,\rho) = 1$ for all values of ρ [5]. One notices that $\overline{\delta}_l$ is real, since the Coulomb functions are real. Moreover, it vanishes inside the barrier for narrow resonant states due to very small values of the regular Coulomb function, i.e. in this region it is $e^{2i\overline{\delta}_l(E,R)} \approx 1$.

2.3.2 Resonances

Close to the resonant energy E_n one can expand the logarithmic derivative as follows

$$\beta_l^{(\mathrm{int})}(E,R) \approx \beta_l(E_n,R) + \beta_l'(E_n,R)(E - E_n), \tag{2.38}$$

and the S-matrix becomes

$$\mathscr{S}_{nl}(E,R) = e^{2i\bar{\delta}_l(E,R)}\frac{E - E_n - \Delta_{nl}(E,R) - \frac{i}{2}\Gamma_{nl}(E,R)}{E - E_n - \Delta_{nl}(E,R) + \frac{i}{2}\Gamma_{nl}(E,R)} \tag{2.39}$$

where we introduced the energy shift and decay width as

$$\begin{aligned}\Delta_{nl}(E,R) &\equiv \frac{D_l(E,R) - \beta_l(E_n,R)}{\beta_l'(E_n,R)},\\ \Gamma_{nl}(E,R) &\equiv -\frac{2P_l(E,R)}{\beta_l'(E_n,R)}.\end{aligned} \tag{2.40}$$

In order to estimate the derivative of the logarithmic derivative with respect to the energy we consider two internal solutions of Eq. 2.65, namely $f_1(r) \equiv f_l(E_1, r)$ and $f_2(r) \equiv f_l(E_2, r)$. Since they obey the Schrödinger equation one gets

$$f_2(r)\frac{d^2f_1(r)}{dr^2} - f_1(r)\frac{d^2f_2(r)}{dr^2} = \frac{2\mu}{\hbar^2}(E_2 - E_1)f_1(r)f_2(r). \tag{2.41}$$

By integrating both sides from 0 to R, dividing by $f_1(R)f_2(R)$ and using the fact that the internal solution should be regular in origin, i.e. $f_l(E, r = 0) = 0$, one obtains

$$\begin{aligned}&\frac{R}{f_1(R)}\frac{df_1(R)}{dr} - \frac{R}{f_2(R)}\frac{df_2(R)}{dr} = \beta(E_1,R) - \beta(E_2,R)\\ &= (E_2 - E_1)\frac{2\mu R}{\hbar^2 f_1(R)f_2(R)}\int_0^R f_1(r)f_2(r)dr.\end{aligned} \tag{2.42}$$

In the limit $E_2 \to E_1 = E$ and normalizing to unity the internal wave function one gets

$$-\frac{d}{dE}\beta_l(E,R) = \frac{2\mu R}{\hbar^2 f_l^2(E,R)} \equiv \gamma_l^{-2}(E,R), \tag{2.43}$$

where we introduced the reduced width γ_l. Thus, the decay width in Eq. 2.40 acquires the standard form, as a product between the penetrability and reduced width squared, i.e.

$$\Gamma_{nl}(E,R) = 2P_l(E,R)\gamma_l^2(E_n,R), \tag{2.44}$$

which is a real positive number. We will see later that the same factorization of the decay width is also given by the R-matrix theory [6].

According to Eq. 2.39 the maximum value of the S-matrix occurs when the denominator is a minimun, i.e. for the energy $E = E_{nl}^{(0)}(E,R) = E_n + \Delta_l(E,R)$. In terms of this energy the S-matrix reads

$$\mathscr{S}_{nl}(E,R) = e^{2i\overline{\delta}_l(E,R)}\frac{E - E_{nl}^{(0)}(E,R) - \frac{i}{2}\Gamma_{nl}(E,R)}{E - E_{nl}^{(0)}(E,R) + \frac{i}{2}\Gamma_{nl}(E,R)}. \tag{2.45}$$

Physically, this equation is interpreted as the S-matrix corresponding to a resonance with energy $E_{nl}^{(0)}(E,R)$ and width $\Gamma_{nl}(E, R)$.

So far we have been careful to show the dependence upon E and R of the parameters entering the S-matrix, i.e. $E_{nl}^{(0)}(E,R)$ and $\Gamma_{nl}(E, R)$. However it has to be stressed that the dependence upon R is artificial, since the theory should not depend upon the matching radius if this point is properly chosen, i.e. beyond the range of the nuclear force. The dependence upon the energy, based in the approximation (2.38), is a more serious point. Wigner realized that this dependence is irrelevant in the analysis of observable resonances, since in that case the width is so small that in the energy range of the resonance Γ can be considered a constant. In the rest of this section we will only consider narrow resonances. That is the S-matrix has the form

$$\mathscr{S}_{nl}(E) = e^{2i\overline{\delta}_l}\frac{E - E_{nl}^{(0)} - \frac{i}{2}\Gamma_{nl}}{E - E_{nl}^{(0)} + \frac{i}{2}\Gamma_{nl}} = e^{2i\overline{\delta}_l}\left[1 - \frac{i\Gamma_{nl}}{E - E_{nl}^{(0)} + \frac{i}{2}\Gamma_{nl}}\right]. \tag{2.46}$$

where $E_{nl}^{(0)}$ and Γ_{nl} are real positive numbers.

It is important to keep in mind that Eq. 2.46 was obtained by assuming that Γ_{nl} is small and therefore it is only valid for narrow (and therefore isolated) resonances.

2.3.3 Poles of the S-Matrix

The poles of the S-matrix characterize the type of the resonant state. From Eq. 2.46 one sees that the energies and widths of narrow resonances can be obtained by calculating the complex poles of the S-matrix. But this is a very difficult task, because Γ_l can be many orders of magnitude smaller than $E_l^{(0)}$ and the computation of the complex energy $E_l^{(0)} + i\Gamma_l/2$ would require a very high precision. We will come back to this problem in Sect.2.4. But still one can compute the energy of the resonance as the pole of the S-matrix and then the width as the corresponding residues. To see this, we first notice that the number $\overline{\delta}_l$ (called "hard sphere phase shift") represents the contribution of the continuum background to the S-matrix and its value is negligible close to a narrow resonance. Therefore, the residues of the S-matrix at the pole n is

$$\mathrm{Res}[\mathscr{S}_{nl}(E)] = \lim_{E \to E_{nl}^{(0)} - \frac{i}{2}\Gamma_{nl}} \left(E - E_{nl}^{(0)} + \frac{i}{2}\Gamma_{nl}\right)\mathscr{S}_{nl}(E) = -i\Gamma_{nl}, \tag{2.47}$$

which is an important result since it shows that if the resonance is isolated then the residues of the S-matrix is a pure imaginary number. On the contrary, for resonances that are not isolated the residua are generally complex quantities [7].

Let us mention that by exchanging $H_l^{(+)}$ and $H_l^{(-)}$ between them in Eq. 2.31 one obtains a symmetric pole. Thus, by writing

$$\kappa_{nl} = \kappa_{nl}^{(0)} - i\lambda_{nl}, \tag{2.48}$$

where $\lambda_{nl} = \Gamma_{nl}/2$ the poles of the S-matrix are [8, 9]:

(a) decay states (Gamow resonances) with $\kappa_{nl}^{(0)} > 0$, $\lambda_{nl} > 0$ (dark squares in Fig. 2.2);
(b) capture states with $\kappa_{nl}^{(0)} < 0$, $\lambda_{nl} > 0$ (open squares in Fig. 2.2).

Let us mention that for negative energies the S-matrix has only imaginary poles, corresponding in (2.25) to the following asymptotics

$$f_l(\rho) \rightarrow exp[\mp(\rho + \frac{1}{2}l\pi)], \tag{2.49}$$

These are

(c) bound states, for which $\kappa_{nl}^{(0)} = 0$ and $\lambda_{nl} < 0$ (dark circles in Fig. 2.2);
(d) antibound states with $\kappa_{nl}^{(0)} = 0$, $\lambda_{nl} > 0$ (open circles in Fig. 2.2).

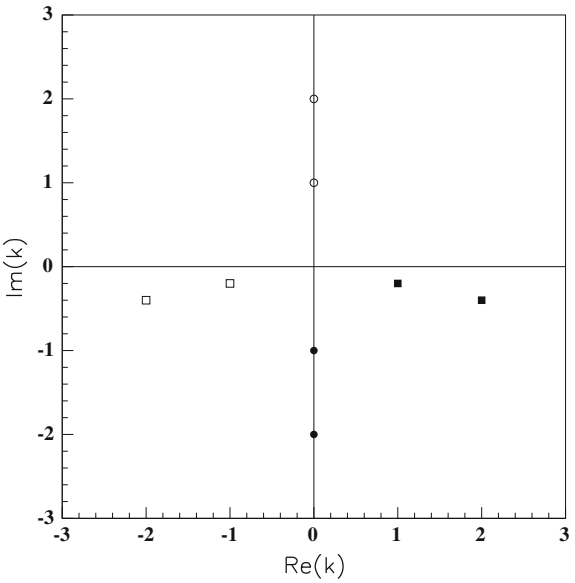

Fig. 2.2 Poles of the S-matrix: bound states (*dark circles*), antibound states (*open circles*), decay states (*dark squares*), capture states (*open squares*)

From Eq. 2.46 one also obtains

$$\delta_{nl} = \arctan\frac{\Gamma_{nl}/2}{E_{nl}^{(0)} - E}, \tag{2.50}$$

which shows that a resonance appears when the phase shift increases as it approaches the value $\delta_{nl} = \pi/2$ as a function of the energy assuming, also here, that the hard sphere phase shift is negligible. This criterion is often used to determine the energies of resonances.

Equation 2.50 allows one to evaluate the decay width by using still another expression, namely

$$\Gamma_{nl} = -2\left[\frac{\partial ctg\,\delta_{nl}}{\partial E}\right]^{-1}_{E=E^0_{nl}}. \tag{2.51}$$

Finally, it is worthwhile to mention that from Eq. 2.46 the cross section corresponding to the scattering of the particle at the energy of the resonance acquires the form

$$\sigma_{nl}(E) = (2l+1)\frac{\pi}{k^2}\frac{\Gamma_{nl}^2}{(E - E_{nl}^{(0)})^2 + (\Gamma_{nl}/2)^2}. \tag{2.52}$$

This formula was derived by G. Breit and E. P. Wigner [10] to explain the capture of slow neutrons. It is one of the most successful expressions written in quantum physics, as shown by its extensive use in the study of resonances ever since. It was by comparing with the experiment Wigner interpreted the number Γ as the width of the resonance. Since the imaginary part of the S-matrix pole is $-\Gamma/2$ (Eq. 2.46), this interpretation coincided with the Gamow interpretation of the width.

2.4 Gamow States

The states with complex energies $E = E_l^{(0)} - \frac{i}{2}\Gamma_l$, corresponding to the poles of the type (a) and (b), are called Gamow outgoing/ingoing states. According to the representation of the S-matrix (2.45) the scattering state (2.31) is given by

$$\begin{aligned} f_l^{(\mathrm{ext})}(r) \sim &\left(E - E_l^{(0)} + \frac{i}{2}\Gamma_l\right) H_l^{(\mp)}(\chi, \rho) \\ &- \left(E - E_l^{(0)} - \frac{i}{2}\Gamma_l\right) H_l^{(\pm)}(\chi, \rho), \end{aligned} \tag{2.53}$$

and the first term vanishes. Thus, the Gamow states are eigenstates of the stationary system of equations (2.14) with the following asymptotics

$$f_l^{(\mathrm{ext})}(r) = N_l H_l^{(\pm)}(\chi, \rho). \tag{2.54}$$

We can now formulate the complex eigenvalue problem for the Gamow states. The internal component of the relative wave function $f_l^{(\mathrm{int})}(r)$ should be regular in origin (2.34). The continuity of logarithmic derivatives for the internal and external wavefunction component of the resonant type (2.54) at some large radius R, where the interaction is given by the spherical Coulomb potential, can be fulfilled only for a discrete set of complex values of the wave number κ_{nl} (2.48), given by the above cases (a) and (b).

The angular momentum representation can be generalized for deformed nuclei, where both emitted fragments have structure and they can be left in some excited states. The dynamics of the decaying system is described by the following stationary Schrödinger equation

$$\mathbf{H}\Psi_{J_iM_i}(\mathbf{x_1},\mathbf{x_2},\mathbf{r}) = E\Psi_{J_iM_i}(\mathbf{x_1},\mathbf{x_2},\mathbf{r}). \tag{2.55}$$

We consider that the Hamiltonian describing binary emission is given by the following general ansatz

$$\mathbf{H} = -\frac{\hbar^2}{2\mu}\Delta_r + \mathbf{H}_1(\mathbf{x_1}) + \mathbf{H}_2(\mathbf{x_2}) + V(\mathbf{x_1},\mathbf{x_2},\mathbf{r}), \tag{2.56}$$

where $\mathbf{x}_k$ denote the internal coordinates of fragments and $\mathbf{r}$ the distance between them. We denote by V the inter-fragment potential and by $\mathbf{H}_k$ the Hamiltonians describing the internal motion of emitted fragments, i.e.

$$\mathbf{H}_k\Phi_{J_kM_k}(\mathbf{x}_k) = E_k\Phi_{J_kM_k}(\mathbf{x}_k), = 1,2, \tag{2.57}$$

where E_k are the excitation energies of emitted fragments and $\Phi_{J_kM_k}(\mathbf{x}_k)$ their eigenstates, satisfying the orthonormality condition

$$\langle\Phi_{J_kM_k}|\Phi_{J'_kM'_k}\rangle = \delta_{J_kJ'_k}\delta_{M_kM'_k}. \tag{2.58}$$

The external solution can be written as a superposition of different outgoing channels $c \equiv (J_1, J_2, J_c, j_c)$, describing all possible binary splittings, i.e.

$$\Psi_{J_iM_i}(\mathbf{x_1},\mathbf{x_2},\mathbf{r}) = \sum_c \Psi^{(c)}_{J_iM_i}(\mathbf{x_1},\mathbf{x_2},\mathbf{r}) = \sum_c \frac{f_c(r)}{r}\mathscr{Y}^{(c)}_{J_iM_i}(\mathbf{x_1},\mathbf{x_2},\hat{r}), \tag{2.59}$$

where, with $\hat{r} \equiv (\phi,\theta)$, we introduced the core-angular harmonics

$$\langle\mathbf{x_1},\mathbf{x_2},\hat{r}|c\rangle \equiv \mathscr{Y}^{(c)}_{J_iM_i}(\mathbf{x_1},\mathbf{x_2},\hat{r}) = \left\{[\Phi_{J_1}(\mathbf{x_1})\otimes\Phi_{J_2}(\mathbf{x_2})]_{J_c}\otimes\mathscr{Y}_{j_c}(\hat{r})\right\}_{J_iM_i}. \tag{2.60}$$

As usually, the symbol $[... \otimes ...]_{JM}$ denotes the angular momentum coupling. Thus, the total spin is decomposed in each channel as follows

$$\begin{aligned}\mathbf{J}_i &= \mathbf{J}_c + \mathbf{j}_c\\ \mathbf{J}_c &= \mathbf{J}_1 + \mathbf{J}_2.\end{aligned} \tag{2.61}$$

These functions are also introduced within the R-matrix theory [6, 11, 12], were they are called surface functions. Obviously when one of the emitted fragments is structureless, like for instance in proton or α emission, one has $\Phi_{J_2}(\mathbf{x}_2) = 1$. The harmonics $\mathscr{Y}_{j_c m_c}(\hat{r})$ describe the angular relative motion and they coincide with usual spherical harmonics (2.10) in the case both fragments are bosons. Here j_c is an integer number. They coincide with spin-orbital harmonics (2.28) for the fermion (proton or neutron) emission, where j_c is half integer.

Due to the orthonormality of their components, the core-angular harmonics are mutually orthonormal, i.e.

$$\langle c|c'\rangle = \langle \mathscr{Y}^{(c)}_{J_i M_i} | \mathscr{Y}^{(c')}_{J_i M_i} \rangle = \delta_{cc'}. \tag{2.62}$$

We split the inter-fragment potential into a spherical and a deformed component, i.e. $V = V_0 + V_d$. By projecting out a given channel c and taking into account the orthonormality condition (2.62) one obtains the coupled channels system of equations for the radial wave functions

$$\frac{d^2 f_c(r)}{dr^2} = \left\{ \frac{l_c(l_c+1)}{r^2} + \frac{2\mu}{\hbar^2}[V_0(r) - E_c] \right\} f_c(r) + \frac{2\mu}{\hbar^2} \sum_{c'} V_d^{(cc')}(r) f_{c'}(r), \tag{2.63}$$

where the channel energy is defined as $E_c = E - E_1 - E_2$ and

$$V_d^{(cc')}(r) = \langle \mathscr{Y}^{(c)}_{J_i M_i} | V_d | \mathscr{Y}^{(c')}_{J_i M_i} \rangle. \tag{2.64}$$

At large distances only the spherical component is dominant and therefore the above system becomes decoupled

$$\left[-\frac{d^2}{d\rho_c^2} + \frac{l_c(l_c+1)}{\rho_c^2} + \frac{V_0(r)}{E_c} - 1 \right] f_c(r) = 0, \tag{2.65}$$

in terms of the reduced radius for a given channel "c" $\rho_c = \kappa_c r$, where momentum is defined by $\kappa_c = \sqrt{2\mu E_c}/\hbar$. Here one has only the spherical Coulomb interaction (2.17) and the system (2.65) has a similar to (2.20) form for each angular momentum in the channel c, i.e.

$$\left[-\frac{d^2}{d\rho_c^2} + \frac{l_c(l_c+1)}{\rho_c^2} + \frac{\chi_c}{\rho_c} - 1 \right] f_c(\chi_c, \rho_c) = 0, \tag{2.66}$$

where the channel Coulomb parameter is given by

$$\chi_c = 2\frac{Z_1 Z_2 e^2}{\hbar v_c}, \tag{2.67}$$

with the asymptotic channel velocity defined as follows

$$v_c = \sqrt{\frac{2E_c}{\mu}} = \frac{\hbar \kappa_c}{\mu}. \tag{2.68}$$

The outgoing/ingoing solutions of Eq. 2.66 are the standard Coulomb–Hankel waves (2.24). Thus, the general solution is an eigenstate of the stationary system of equations (2.63) with the following asymptotics

$$f_c(r) \rightarrow_{r\rightarrow\infty} f_c^{(\mathrm{ext})}(r), \tag{2.69}$$

where $f_c^{(\mathrm{ext})}(r)$ satisfies Eq. 2.66, i.e. it is a linear combination of (2.24). As in the spherical case, by denoting with $f_c^{(\mathrm{int})}(r)$ the internal components of the relative wave function regular in the origin, the continuity of the logarithmic derivatives of the wavefunction components at some large radius R, where the interaction becomes spherical, is given by a similar to Eq. 2.35 condition for each channel, i.e.

$$\beta_c^{(\mathrm{int})}(R) \equiv \frac{1}{f_c^{(\mathrm{int})}(R)} \frac{df_c^{(\mathrm{int})}(R)}{dr} = \beta_c^{(\mathrm{ext})}(R) \equiv \frac{1}{f_c^{(\mathrm{ext})}(R)} \frac{df_c^{(\mathrm{ext})}(R)}{dr}. \tag{2.70}$$

It can be fulfilled only for a discrete set of complex values of the wave number κ_n for the above (a)–(d) cases.

As in the spherical case, the cases (a) and (b) are respectively satisfied by the following asymptotics

$$f_c^{(\mathrm{ext})}(r) = N_c H_{l_c}^{(\pm)}(\chi_c, \rho_c), \tag{2.71}$$

where N_c are the scattering amplitudes in the channel c.

2.5 Decay Width and Half Life

For Gamow states (a) the imaginary part of κ according to (2.7) is negative and the modulus of the outgoing wave increases at large distances. By considering Eqs. 2.6 and 2.7, one obtains that the matter density decreases according to the following rule

$$|\Phi(t, \mathbf{r})|^2 = |\Psi(\mathbf{r})|^2 e^{-\Gamma t/\hbar}, \tag{2.72}$$

which is nothing else but the well-known exponential decay law, giving the number of nuclei at a certain moment

$$N(t) = N(0)e^{-\lambda t}, \tag{2.73}$$

where the decay constant is given by $\lambda = \Gamma/\hbar$. The half life is defined as the interval of time satisfying the condition $N(T) = N(0)/2$, i.e.

$$T_{1/2} = \frac{\hbar \ln 2}{\Gamma} = \frac{4.56 \times 10^{-22}}{\Gamma}, \tag{2.74}$$

where Γ is in MeV and T in seconds.

The decay width can be determined, in principle, by solving the coupled channels system (2.63) with the matching conditions (2.70) in the complex energy plane. The evaluation of the S-matrix poles can be performed by using the same procedure as the one used to evaluate bound states. The difference is that, now, one has to introduce the outgoing boundary condition given by Eq. 2.71. There are standard computer codes to do this, e.g. the codes of Refs. [13, 14]. These codes evaluate the energies corresponding to all poles of the S-matrix. The real energies define either the bound, or the antibound states. The complex energies, which are close to the real energy axis correspond to narrow resonances and therefore they accept the interpretation given above to such energies. That is, the real part is the position of the decaying resonance and minus twice the imaginary part is the corresponding width. However, in observable emission processes, the value of the imaginary part is usually much smaller, in absolute value, than the corresponding real part and its calculation is a difficult numerical task. But even if this calculation is possible, we want to stress that not always does the imaginary part of the energies correspond to the width of a resonance.

There is also an equivalent way to determine the width. Let us consider the stationary Schrödinger equation and its complex conjugate

$$\begin{aligned}\left(E-\frac{i}{2}\Gamma\right)\Psi&=\left(-\frac{\hbar^2}{2\mu}\nabla^2+V\right)\Psi\\ \left(E+\frac{i}{2}\Gamma\right)\Psi^*&=\left(-\frac{\hbar^2}{2\mu}\nabla^2+V\right)\Psi^*.\end{aligned}\tag{2.75}$$

One multiplies to the left the first relation by Ψ^* and the second one by Ψ. By substracting the two equalities one obtains

$$\Gamma\Psi^*\Psi=\frac{\hbar^2}{2\mu i}\left(\Psi^*\nabla^2\Psi-\Psi\nabla^2\Psi^*\right).\tag{2.76}$$

Here we considered that the potential operator V is Hermitian and therefore the corresponding difference vanishes after the volume integration. We then integrate this relation over internal variables $\mathbf{x}_1$, $\mathbf{x}_2$ and the relative coordinate $\mathbf{r}$ inside a sphere with a large radius. By transforming the right hand side term into a surface integral one obtains the following expression of the decay width

$$\Gamma=\frac{\hbar\oint\mathscr{J}(\hat{r})d\hat{r}}{\int\mathscr{P}(\mathbf{r})d\mathbf{r}}.\tag{2.77}$$

Here we introduced the internal probability

$$\mathscr{P}(\mathbf{r})=\int d\mathbf{x}_1\int d\mathbf{x}_2|\Psi|^2,\tag{2.78}$$

and the probability flux

$$\mathcal{J}(\hat{r}) = \frac{\hbar}{2\mu i}\int d\mathbf{x}_1 \int d\mathbf{x}_2 (\Psi^* \nabla \Psi - \Psi \nabla \Psi^*) r^2. \tag{2.79}$$

We consider that the wave function is normalized to unity inside the considered sphere. In this way we suppose that the two fragments exist with the unity probability inside this volume. This statement is in an aparent contradiction with the emission process, leading to a decrease of the internal probability. Anyway, due to the very small value of the decay width compared with the emission energy one can use this condition, for a relative large time interval compared with the characteristic nuclear time [15].

On the surface of the sphere the gradient operator acts only on the radial direction $\nabla \rightarrow \mathbf{e}_r \frac{\partial}{\partial r}$, i.e.

$$\mathcal{J}(\hat{r}) \rightarrow \frac{\hbar}{2\mu i}\int d\mathbf{x}_1 \int d\mathbf{x}_2 \left(\Psi^* \frac{\partial \Psi}{\partial r} - \Psi \frac{\partial \Psi^*}{\partial r}\right) r^2. \tag{2.80}$$

Thus, by using the channel expansion (2.59) and

$$\frac{\partial \Psi^{(c)}}{\partial r} \rightarrow i\kappa_c \Psi^{(c)}, \tag{2.81}$$

the angular distribution becomes

$$\Gamma(\hat{r}) = \hbar \mathcal{J}(\hat{r}) = \hbar \sum_{cc'} v_c \lim_{r\rightarrow\infty} r^2 \int d\mathbf{x}_1 \int d\mathbf{x}_2 \Psi^{(c)*} \Psi^{(c')}. \tag{2.82}$$

By using the orthogonality of the core-angular harmonics (2.62) the decay width, proportional to the total probability flux through the surface of this sphere, becomes

$$\Gamma = \oint \Gamma(\hat{r}) d\hat{r} = \hbar \sum_c v_c \lim_{r\rightarrow\infty} \oint r^2 d\hat{r} \int d\mathbf{x}_1 \int d\mathbf{x}_2 |\Psi^{(c)}|^2. \tag{2.83}$$

By using the asymptotic relation (2.71) and the fact that the modulus of the outgoing Coulomb–Hankel wave function is unity, as seen from Eq. 2.24, one obtains

$$\Gamma = \sum_c \hbar v_c |N_c|^2 \equiv \sum_c \Gamma_c. \tag{2.84}$$

Thus, the total decay width can be written as a sum of partial decay widths corresponding to the considered channels. The equality between internal and external radial wave functions together with Eq. 2.71, i.e.

$$f_c^{(\mathrm{int})}(E_c, R) = f_c^{(\mathrm{ext})}(E_c, R) = N_c H_{l_c}^{(+)}(\chi_c, \kappa_c R), \tag{2.85}$$

determines the scattering amplitude

$$N_c = \frac{f_c^{(\mathrm{int})}(E_c, R)}{H_{l_c}^{(+)}(\chi_c, \kappa_c R)}. \tag{2.86}$$

Notice that N_c does not depend upon R, since both internal and external components satisfy the same Schrödinger equation. By inserting this value in the expression of the decay width (2.83) one obtains the following relation

$$\Gamma_c = \hbar v_c \left| \frac{f_c^{(\mathrm{int})}(E_c, R)}{H_{l_c}^{(+)}(\chi_c, \kappa_c R)} \right|^2 = 2P_{l_c}(E_c, R)\gamma_c^2(E_c, R), \tag{2.87}$$

where χ_c is the Coulomb parameter corresponding to the resonant complex energy. Here we introduced the standard penetrability and reduced width squared [6]

$$\begin{aligned} P_{l_c}(E_c, R) &= \frac{\kappa_c R}{\left| H_{l_c}^{(+)}(\chi_c, \kappa_c R) \right|^2}, \\ \gamma_c^2(E_c, R) &= \frac{\hbar^2}{2\mu R} |f_c^{(\mathrm{int})}(E_c, R)|^2. \end{aligned} \tag{2.88}$$

The form of the above decay width at the energy $E = E_c$, in terms of the penetrability and reduced width, is the same as in Eq. 2.44.

2.6 Decay Rules for the Half Life

According to the factorization of the decay width (2.87) and the above relation for the penetrability (2.88) the half life (2.74) is proportional to the modulus squared of the Coulomb–Hankel function inside the barrier. In this region it practically coincides with the irregular Coulomb function and has a very simple WKB ansatz, given in Appendix (14.2) by

$$\begin{aligned} H_l^{(+)}(\chi, \rho) &\approx (ctg\,\alpha)^{1/2} exp[\chi(\alpha - \sin\alpha\cos\alpha)] C_l \\ &= \left(\frac{1}{x} - 1\right)^{-1/4} exp\left[\chi\left(\arccos\sqrt{x} - \sqrt{x(1-x)}\right)\right] C_l \\ &\equiv H_0^{(+)}(\chi, \rho) C_l \end{aligned} \tag{2.89}$$

where, with the external turning point $R_b = Z_1 Z_2 e^2/E$ and barrier energy $V_0 = Z_1 Z_2 e^2/R$, we introduced the following notations

$$\cos^2\alpha = x = \frac{\rho}{\chi} = \frac{R}{R_b} = \frac{E}{V_0}$$
$$C_l = exp\left[\frac{l(l+1)}{\chi}\sqrt{\frac{\chi}{\rho}-1}\right]. \tag{2.90}$$

Thus, the logarithm of the half life, corrected by the exponential centrifugal factor C_l defined by the second line of this relation, should be proportional to the Coulomb parameter, i.e.

$$\log_{10} T_{\rm red} = a_0\chi + b_0, \tag{2.91}$$

where we defined the reduced half life by

$$T_{\rm red} = \frac{T_{1/2}}{C_l^2} = \frac{\ln 2}{v_l}\left|\frac{H_0^{(+)}(\chi,\rho)}{f_l^{(\rm int)}(R)}\right|^2. \tag{2.92}$$

This relation is also called Geiger–Nuttall law, discovered in 1911 [16, 17] for α-decay between ground states (where the angular momentum carried by the α-particle is $l = 0$) and it can be written as follows

$$\log_{10} T_{1/2} = a\frac{Z}{\sqrt{Q_\alpha}} + b, \tag{2.93}$$

where Z is the charge of the left daughter nucleus and Q_α the Q-value of the α-particle. As we pointed out the explanation of this law was given by G. Gamow in 1928 [2], in terms of the quantum-mechanical penetration of the Coulomb barrier, given by the first line of Eq. 2.88. This quantity is characterized by the Coulomb parameter, which is proportional to the ratio $Z/\sqrt{Q_\alpha}$.

A special situation occurs in the case of proton emission, when the angular momentum of the emitted proton in general is different from zero. The half lives systematics for known proton emitters [18, 19, 20] is given in Fig. 2.3a. The picture becomes much simpler for the reduced half life (2.92) in Fig. 2.3b.

The Geiger–Nuttall law for proton emitters can be reproduced by the formula

$$log_{10} T_{red}^{(k)} = a_k(\chi - 20) + b_k,$$
$$a_1 = 1.31, \quad b_1 = -2.44, \quad Z < 68 \tag{2.94}$$
$$a_2 = 1.25, \quad b_2 = -4.71, \quad Z > 68,$$

where $k = 1$ corresponds to the upper line in Fig. 2.3b. The standard errors are $\sigma_1 = 0.26$ and $\sigma_2 = 0.23$, corresponding to a mean factor less than two. Here we considered the geometrical radius, i.e. $R = 1.2(A_D^{1/3} + 1)$. We will give in the next Section the explanation for this specific form of the Geiger–Nuttall law for proton emitters.

The two-proton emission was predicted in 1960 [21], but at the moment, the experimental material consists of few cases only. In Fig. 2.4, it is shown the

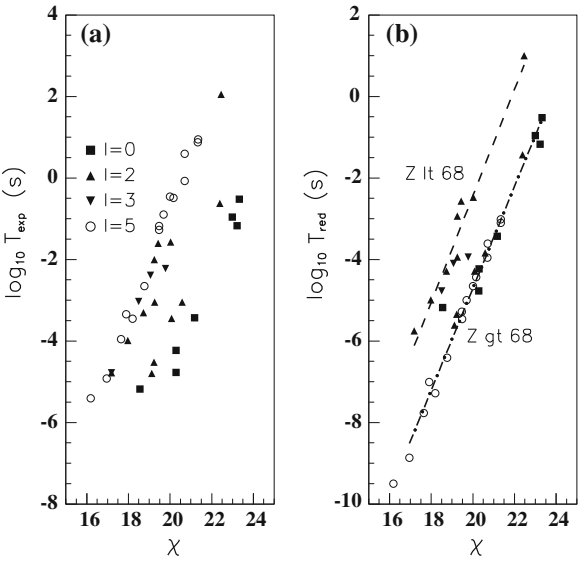

Fig. 2.3 **a** Logarithm of half lives for proton emitters versus the Coulomb parameter (2.67). *Different symbols* denote angular momenta carried by the emitted proton. **b** Logarithm of reduced half lives (2.92) for proton emitters versus the Coulomb parameter

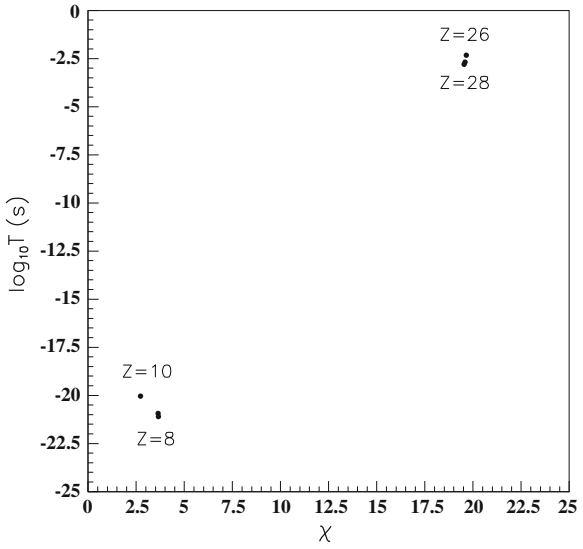

Fig. 2.4 Logarithm of half lives for two-proton emitters versus the Coulomb parameter (2.67). The charge of the mother nucleus is indicated

logarithm of the half life versus the Coulomb parameter, by considering a di-proton emission.

The α-decays between ground states are characterized by a remarkable regularity, especially for transitions between ground states of even–even nuclei. The logarithm of half lives along various isotopic chains lie on separate lines, as it is shown in Fig. 2.5. This feature is known as the Viola–Seaborg rule [22], i.e.

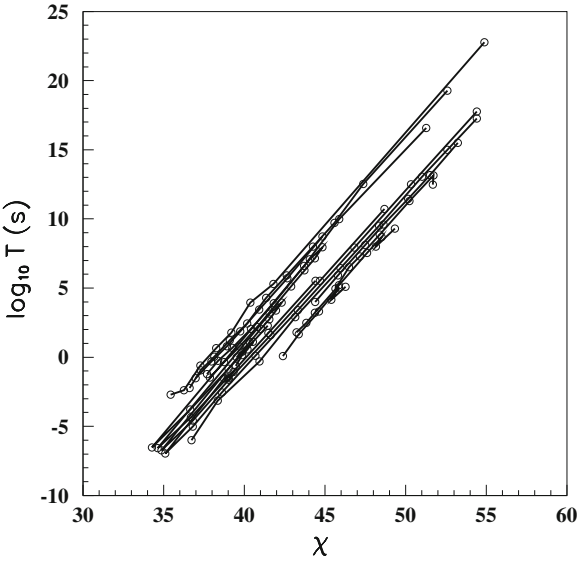

Fig. 2.5 Logarithm of half lives for α-decays from even–even nuclei versus Coulomb parameter (2.67). *Different lines* connect decays from nuclei with the same charge number

$$\log_{10} T_{1/2} = \frac{a_1 Z + a_2}{\sqrt{Q_\alpha}} + b_1 Z + b_2, \tag{2.95}$$

and it is connected with different α-particle reduced widths, multiplying the penetrability in (2.87), as will be shown latter. Still in doing systematics along neutron chains, there are important deviations with respect to this rule, as for instance in α-decay from odd mass nuclei, and this feature is strongly connected with nuclear structure details.

By using Eq. 2.89 a semi-empirical α-decay universal law for even–even emitters can be written as follows

$$\begin{aligned} \log_{10} T_{1/2} &= -\log_{10} P_\alpha - 20.446 + C(Z,N) \\ -\log_{10} P_\alpha &= A(Z,N)\sqrt{\frac{A_D}{A_P Q_\alpha}}[\arccos\sqrt{X} - \sqrt{X(1-X)}] \\ X &= \frac{R_t}{R_b},\ \ R_t = 1.2249(A_D^{1/3} + 4^{1/3}),\ \ R_b = \frac{2Z_D e^2}{Q_\alpha}, \end{aligned} \tag{2.96}$$

where the functions $A(Z, N)$ and $C(Z, N)$ in terms of the parent proton and neutron numbers are given in Ref. [23].

In Ref. [24] a simpler universal law for even–even α-emitters is given by

$$\log_{10} T_{1/2} = 9.54\frac{Z_D^{0.6}}{\sqrt{Q_\alpha}} - 51.37. \tag{2.97}$$

Recently in Ref. [25] another type of law, taking into account all relevant dependencies, was proposed

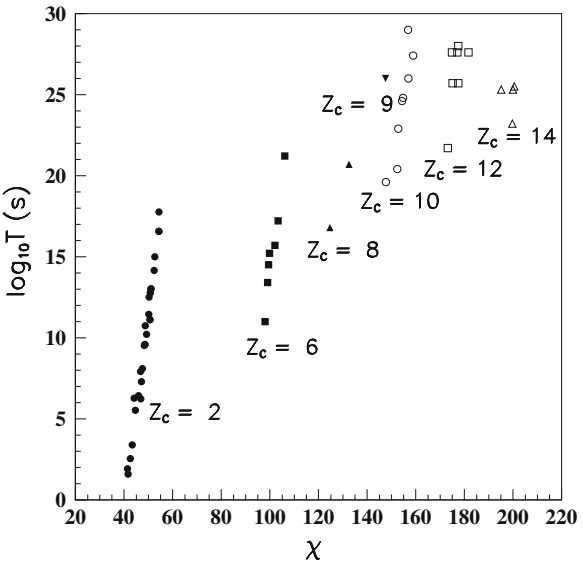

Fig. 2.6 Logarithm of half lives for heavy cluster decays and the corresponding α-decays from the same mother nuclei versus Coulomb parameter (2.67). *Different symbols* denote charge number of the emitted cluster

$$\log_{10}T_{1/2} = a + b\frac{A^{1/6}Z^{1/2}}{\mu} + c\frac{Z}{\sqrt{Q_\alpha}} + d\frac{A^{1/6}\sqrt{l(l+1)}}{Q_\alpha} + e[(-)^j - 1], \qquad (2.98)$$

where A and Z are the parent mass and charge numbers respectively, with different sets of parameters for even–even, odd–odd, even–odd and odd–even α-emitters.

Viola–Seaborg rule can be generalized for heavy-cluster decays [26], as it is shown in Fig. 2.6. Here, the angular momenta carried by emitted fragments are zero. Thus, a similar to Eq. 2.96 universal law for the heavy cluster emission $P \to D + C$ is given by the following ansatz

$$\begin{aligned}
&\log_{10}T_{1/2} = -\log_{10}P_C - 22.169 + 0.598(A_C - 1)\\
&-\log_{10}P_C = 0.22873\sqrt{\mu Z_D Z_C R_b}[\arccos\sqrt{Y} - \sqrt{Y(1-Y)}], \quad \mu = \frac{A_D A_C}{A_P}\\
&Y = \frac{R_t}{R_b}, \;\; R_t = 1.2249(A_D^{1/3} + A_C^{1/3}), \;\; R_b = 1.43998\frac{Z_D Z_C}{Q}.
\end{aligned} \qquad (2.99)$$

By using the expansion in power series of cos α in Eq. 2.89, a simplified version of the above law was recently proposed in Ref. [27], namely

$$\log_{10}T_{1/2} = a\chi' + b\rho' + c, \qquad (2.100)$$

in terms of the following two variables

$$\begin{aligned}
\chi' &= Z_D Z_C\sqrt{A/Q}\\
\rho' &= \sqrt{Z_D Z_C A(A_D^{1/3} + A_C^{1/3})}, \quad A = \frac{A_D A_C}{A_P}.
\end{aligned} \qquad (2.101)$$

In Ref. [28] it was proposed the generalization of the Viola–Seaborg rule for the heavy cluster emission

$$\log_{10} T_{1/2} = a_1 \frac{Z_D Z_C}{\sqrt{Q}} + a_2 Z_D Z_C + b_2 + c_2, \tag{2.102}$$

with the following set of parameters

$$a_1 = 1.517,\ a_2 = 0.053,\ b_2 = -92.911,\ c_2 = 1.402,$$

where c_2 is the blocking parameter for odd-mass nuclei.

Finally, let us mention that it is not possible to derive a Viola–Seaborg rule for cold fission fragments. This feature was evidenced in Ref. [29] by using the Two Center Shell Model described in Sect.12.2. Here, the energy surface of the fissioning system is computed within the liquid drop model plus shell corrections in terms of several coordinates: the distance between emitted fragments, mass asymmetry, deformations and neck coordinate. The double magicity of ^{4}He and ^{208}Pb leads to very pronounced valleys of the total energy surface with a constant mass asymmetry during the whole α-decay of cluster emission process, respectively. Thus, the penetration has a simple expression given by Eq. (2.88), leading to the Viola–Seaborg rule, as we will show in the next section. On the contrary, the cold fission path proceeds through a sadle point of the potential energy surface, close to the double magic nucleus ^{132}Sn, but the mass asymmetry changes during the fission process after this point and the maximum yield corresponds to a different partition. The penetration given by the semiclassical approach (5.2), is computed along the fission path and obviously the half life has a more complex structure which does not satisfy the Viola–Seaborg rule.

Thus, one concludes that all cold emission processes have a common physical root, namely *the cold rearrangement of nucleons during the splitting process to a more stable di-nuclear configuration in which one of fragments has a double-magic structure*.

2.7 Decay Rule for the Reduced Width

The Viola–Seaborg rule (2.95) has a simple explanation in terms of the following schematic cluster-daugher potential [30]

$$\begin{aligned} V(r) &= \hbar\omega \frac{\beta(r - r_0)^2}{2} + v_0,\ r \le r_B \\ &= \frac{Z_D Z_C e^2}{r},\ r > r_B, \end{aligned} \tag{2.103}$$

plotted in Fig. 2.7 for a particular value $r_0 = 0$.

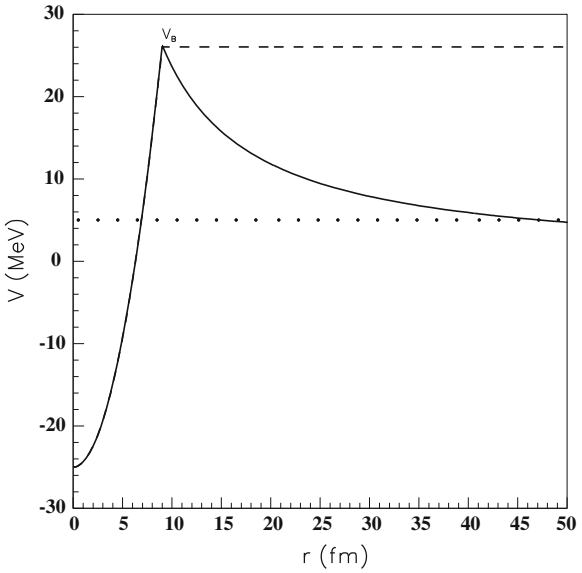

Fig. 2.7 The α-core potential (2.103) with $r_0 = 0$, $v_0 = -25$ MeV (*solid line*) and its barrier value (*dashed line*). Q-value is denoted by a *dotted line*

By considering Q-value as the first eigenstate in a spherical shifted harmonic oscillator well (see Appendix (14.8)), together with the continuity condition at the top of the barrier r_B, i.e.

$$\begin{aligned} Q - v_0 &= \frac{1}{2}\hbar\omega \\ \hbar\omega\frac{\beta(r_B - r_0)^2}{2} + v_0 &= \frac{Z_D Z_C e^2}{r_B}, \end{aligned} \tag{2.104}$$

one obtains the following relation

$$\hbar\omega\frac{\beta(r_B - r_0)^2}{2} = V_{\text{frag}}(r_B) + \frac{1}{2}\hbar\omega, \tag{2.105}$$

where we introduced the so called fragmentation (or driving) potential as the difference between the Coulomb barrier and Q-value

$$V_{\text{frag}}(r_B) = \frac{Z_D Z_C e^2}{r_B} - Q. \tag{2.106}$$

Let us stress on the fact that the above driving potential is a rough estimate of the interaction responsible for the emission process within the two potential model described in Sect. 4.6 in Chap. 4 by Eq. 4.51, i.e. the difference between the dashed and solid lines in Fig. 2.7. As we will show in that Section, this interaction connects the initial bound state to the final state in continuum.

According to Eq. 2.87 the logarithm of the decay width is a sum of two components

$$\log_{10}\Gamma = \log_{10} 2P(r_B) + log_{10}\gamma^2(r_B). \tag{2.107}$$

The first component, in the above relation, contains the logarithm of the Coulomb–Hankel function inside the Coulomb barrier which, according to Eq. 2.89, is proportional to the Coulomb parameter χ. The second part contains the reduced width squared which, according to Eq. 2.88, is proportional to the modulus of the internal wave function squared. For a shifted harmonic oscillator well, one obtains (see Appendix (14.8)) $|f_{\rm int}|^2 = A^2 exp[-\beta(r - r_0)^2]$ and

$$\log_{10}\gamma^2(r_B) = -\frac{log_{10}e^2}{\hbar\omega}V_{\rm frag}(r_B) + \log_{10}\frac{\hbar^2A^2}{2\mu e r_B}. \tag{2.108}$$

Let us stress on the fact that the above relation does not depend upon the radius r_0.

In Fig. 2.8 we plotted the logarithm of the experimental reduced width squared by using Eq. (2.108) versus the neutron number by different open symbols, corresponding to five different regions of even–even α emitters, namely

$$\begin{array}{lll} (1) & Z<82,\ 50\le N<82 & \text{(stars)}, \\ (2) & Z<82,\ 82\le N<126 & \text{(open crosses)}, \\ (3) & Z\ge 82,\ 82\le N<126 & \text{(open circles)}, \\ (4) & Z\ge 82,\ 126\le N<152 & \text{(open squares)}, \\ (5) & Z\ge 82,\ N\ge 152 & \text{(open triangles)}. \end{array} \tag{2.109}$$

In our calculations we used the value of the touching radius, i.e. $r_B = 1.2(A_D^{1/3} + R_C^{1/3})$.

By dark circles in Fig. 2.8, it is given the linear fit of the logarithm of the reduced width squared, in terms of the fragmentation potential (2.106), separately

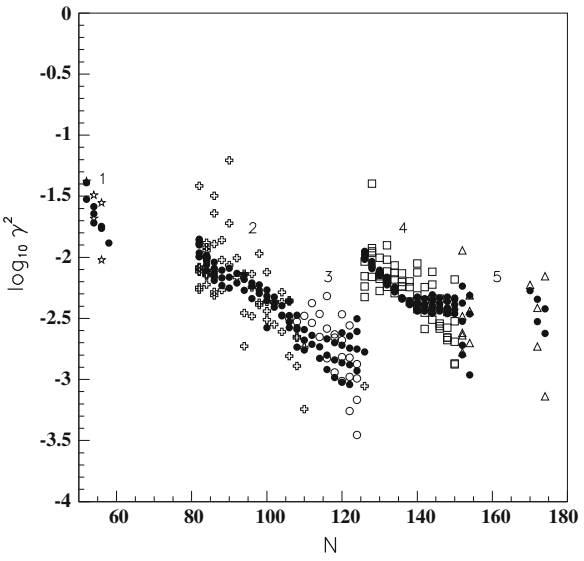

Fig. 2.8 The logarithm of the reduced width squared versus neutron number for five regions of the nuclear chart described by (2.109) (*open symbols*). By *dark circles* are given the results of the linear fit in terms of the fragmentation potential (2.106), separately for each region

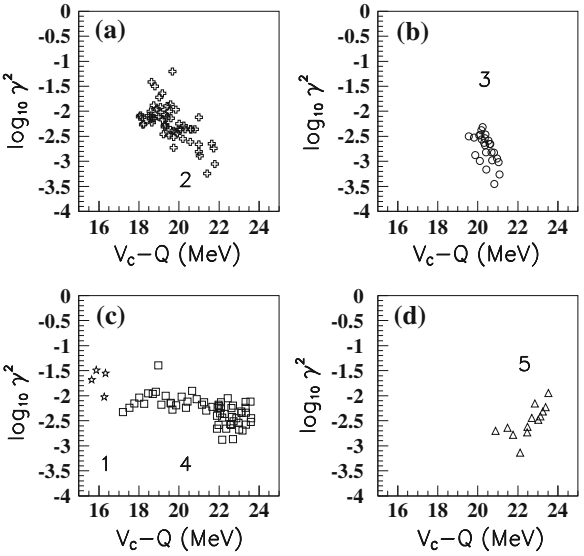

Fig. 2.9 The logarithm of the reduced width squared versus the fragmentation potential (2.106) for five regions of the nuclear chart described by (2.109)

for each region. In order to see this dependence better, in Fig. 2.9 it is given the logarithm of the experimental reduced width versus the fragmentation potential (2.106). Indeed, one sees a nice linear dependence for the regions 1–4, because they contain long isotopic chains, while in the last region 5 one has not more than two isotopes/chain. This is the reason why, except for the last region 5, the reduced width decreases with respect to the fragmentation potential, according to the theoretical prediction given by Eq. 2.108.

In this way one obtains that indeed the logarithm of the half life is of the Viola–Seaborg type

$$\log_{10} T_{1/2} = c_1(r_B)\chi + c_2 V_{\text{frag}}(r_B) + c_3(r_B, A^2), \tag{2.110}$$

because the fragmentation potential contains the product $Z_D Z_C$. Let us mention that in the above relation we neglected for the weaker dependence on the second argument $\rho_B = \kappa r_B = \sqrt{2\mu Q} r_B/\hbar$ of the Coulomb–Hankel function (2.89) [27]. Obviously, the sum does not depend upon the radius and the free term depends on the logarithm of the wave function amplitude squared.

In Fig. 2.10 we plotted the difference $\log_{10} T_{1/2} - c_2 V_{\text{frag}}(r_B) - c_3(r_B, A^2)$ versus the Coulomb parameter χ, by using the same five symbols for the above described regions. Amazingly enough, we obtained three lines, corresponding to different amplitudes of the wave function at the radius r_B. The regions 1 and 4, corresponding to emitters above double magic nuclei ^{50}Sn and ^{208}Pb, respectively, have practically the same internal amplitudes A. The same is true for the regions 3 and 5.

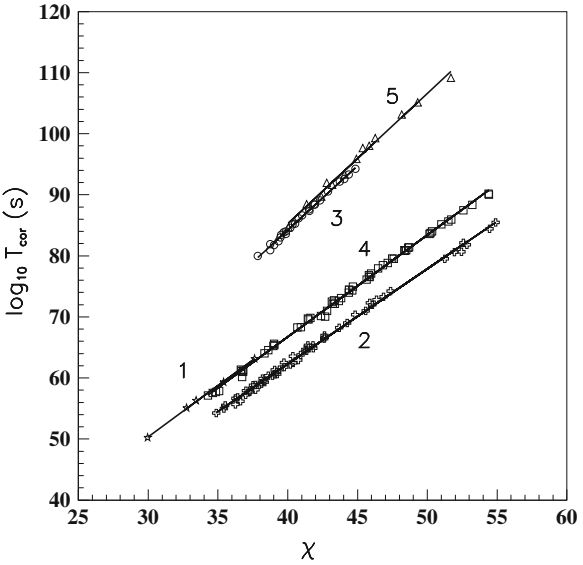

Fig. 2.10 The difference $\log_{10} T_{1/2} - c_2 V_{\text{frag}}(r_B) - c_3(r_B, A^2)$ versus the Coulomb parameter χ for five different regions described by (2.109). The *straight lines* are the corresponding linear fits

Finally we mention that the linear dependence of $\log_{10}\gamma^2$ versus the fragmentation potential (2.108) remains valid for any kind of cluster emission. This fact is nicely confirmed by α and cluster emission processes in Fig. 2.11a, where we plotted the dependence between the corresponding experimental values for the same decays in Fig. 2.6. The straight line is the linear fit for cluster emission processes, except α-decay

$$\log_{10}\gamma^2 = -0.586(V_C - Q) + 15.399. \tag{2.111}$$

As already mentioned, for α-decays the fit gives several parallel lines corresponding to regions (2.109) in Fig. 2.8.

The above value of the slope $-\log_{10} e^2/\hbar\omega$ in Eq. 2.108 leads to $\hbar\omega \approx 1.5$ MeV, with the same order of magnitude as in the α-decay case. The relative large scattering of experimental data around the straight line in Fig. 2.11a can be explained by the simplicity of the used cluster-core potential emission processes, (2.103).

Let us mention that a relation expressing the spectroscopic factor (proportional to the integral of the reduced width squared) for cluster emission processes was derived in Ref. [31]

$$S = S_\alpha^{(A_C-1)/3}, \tag{2.112}$$

where A_C is the mass of the emitted light cluster and $S_\alpha \sim 10^{-2}$. As can be seen from Fig. 2.11b, between A_C and V_{frag} there exists a rather good linear dependence and therefore the above scaling law can be easily understood in terms of the fragmentation potential.

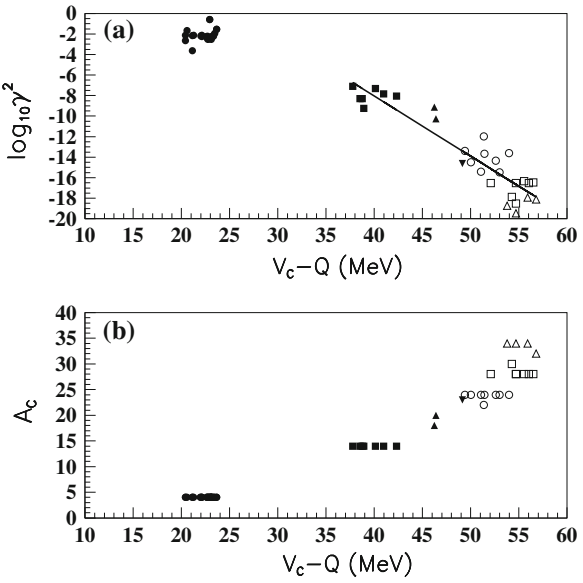

Fig. 2.11 **a** The logarithm of the reduced width squared versus the fragmentation potential (2.106). *Different symbols* correspond to cluster decays in Fig. 2.6. The *straight line* is the linear fit (2.111) for cluster emission processes, except α-decay. **b** Cluster mass number versus the fragmentation potential

Concerning the reduced widths of proton emitters, in Refs. [20, 32] it was pointed out the correlation between the reduced width and the quadrupole deformation. This fact can be seen in Fig. 2.12a, where the region with $Z < 68$ corresponds to $\beta > 0.1$ (open circles), while the other one with $Z > 68$ to $\beta < 0.1$ (dark circles). The two linear fits have obviously different slopes. This dependence is induced by the propagator matrix, entering the definition of the

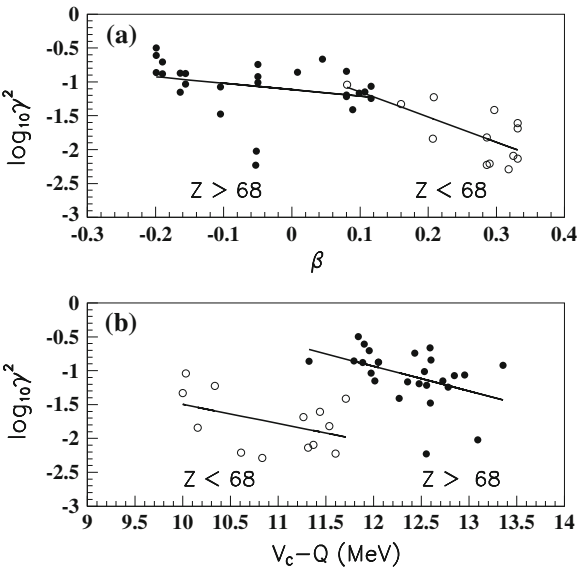

Fig. 2.12 **a** The logarithm of the reduced width squared versus the quadrupole deformation. By *open circles* are given proton emitters with $Z < 68$, while by *dark circles* those with $Z > 68$. The two regression lines fit the corresponding data. **b** The logarithm of the reduced width squared versus the fragmentation potential (2.106). The symbols are the same as in **a**

deformed reduced width, given by Eq. 4.17. Notice that the two dark circles with the smallest reduced widths correspond to the heaviest emitters with $Z > 80$.

At the same time one sees from Fig. 2.12b that the same data are clustered into two regions, which can be directly related with the fragmentation potential (2.106). Here the two linear fits in terms of the fragmentation potential, corresponding to the two regions of charge numbers, have roughly the same slopes, but different values in origin, i.e.

$$\begin{aligned} \log_{10}\gamma^2 &= -0.283(V_C - Q) + 1.329, \quad Z < 68 \\ \log_{10}\gamma^2 &= -0.365(V_C - Q) + 3.440, \quad Z > 68. \end{aligned} \tag{2.113}$$

The ho energy is $\hbar\omega \approx 1.5\,\mathrm{MeV}$ for proton emission, i.e. the same order as for heavy cluster radioactivity and α-decay.

Thus, the two different lines in Fig. 2.3b can be directly connected with similar lines in Fig. 2.12b. They correspond to different orders of magnitude of the fragmentation potential, giving different orders of magnitude to wave functions and therefore to reduced widths.

2.8 Inter-Fragment Potential

As it was already mentioned, we can describe various emission processes, from the proton emission up to the cold fission, within the stationary coupled channels formalism. We suppose that the emitted fragments are already born and their motion is fully described by the Schrödinger equation with a two-body potential, defined for all inter-fragment distances. Obviously, such a description is strictly valid only for the particle (proton/neutron) emission. In the general case when both emitted fragments have structure, like for instance in α-decay, this potential picture is an idealization. Anyway, the emitted fragments are already formed in the region around the geometrical touching point, i.e. at the nuclear surface and only here one can determine a two-body potential. In the overlapping region the Pauli principle acts and the two fragments loose their identity. The equivalent potential becomes non-local and for a correct treatment, it is necessary the antisymmetrization of the wave function within the so-called Resonating Group Method (RGM), as it is described in the review [33], devoted to the microscopic description of cluster emission. Unfortunately, this method is adequate to describe the emission of relative light particle from nuclei close to a double magic nucleus, as it is the α-decay from ^{212}Po.

Anyway, a reasonable way to simulate the Pauli principle is the introduction of a repulsive core. As many calculations showed, the shape of this potential is not important, its only role consists in adjusting the energy of the resonant state in the resulting pocket-like potential to the experimental Q-value. The reason for this is that only the external part of the potential is important, in order to determine the

asymptotics of the wave function and therefore the physical observables, like channel decay widths.

2.9 Double Folding Potential

The most general method to estimate the interaction potential between two composite fragments is the double folding procedure. We will suppose that both emitted fragments can be excited during the decay process. We separate the rotational degrees of freedom from other internal coordinates i.e. $\mathbf{x_k} = (\alpha_k, \omega_k)$, where ω_k are the Euler rotational coordinates. A good approximation of the Hamiltonian, describing the binary emission process, is given by the following ansatz

$$\mathbf{H} = -\frac{\hbar^2}{2\mu}\Delta_r + \mathbf{H}_1(\alpha_1) + \mathbf{H}_2(\alpha_2) + \mathbf{T}_1(\omega_1) + \mathbf{T}_2(\omega_2) + V(\alpha_1, \alpha_2, \omega_1, \omega_2, \mathbf{r}), \tag{2.114}$$

where $\mathbf{H}_k(\alpha_k)$ is connected with the internal dynamics of fragments, while $\mathbf{T}_k(\omega_k)$ with their rotational motion. This Hamiltonian describes a large variety of situations, i.e. proton/neutron emission, α-decay, heavy cluster emission and fission.

The double folding procedure is described in many text-books and review papers, e.g. [34], and consists of the following six dimensional integral

$$\begin{aligned} V(\alpha_1, \alpha_2, \omega_1, \omega_2, \mathbf{r}) &= \int d\mathbf{r}_1 \int d\mathbf{r}_2 \rho_1(\alpha_1, \mathbf{r}_1)\rho_2(\alpha_2, \mathbf{r}_2)v(\mathbf{r}_{12}) \\ \mathbf{r}_{12} &\equiv \mathbf{r} + \mathbf{r}_2 - \mathbf{r}_1, \end{aligned} \tag{2.115}$$

where $\mathbf{r}_k$ is the radius giving the nucleon position inside the k-th nucleus, as seen in Fig. 2.13, ρ_k is the nuclear density of the k-th fragment and $v(\mathbf{r}_{12})$ is the nucleon–nucleon force. The most popular two-body interaction, used to describe heavy ion scattering, is given by a superposition of Yukawa potentials, simulating the exchange of different mesons, called also M3Y interaction [35]. It is given by the following relation

$$v(\mathbf{r}_{12}) = v_{00}(r_{12}) + \hat{J}_{00}\delta(\mathbf{r}_{12}) + v_{01}(r_{12})\boldsymbol{\tau}_1 \cdot \boldsymbol{\tau}_2 + \frac{e^2}{r_{12}}, \tag{2.116}$$

where the central and isospin parts have respectively the following expressions

$$\begin{aligned} v_{00}(r) &= \left[7999\frac{e^{-4r}}{4r} - 2134\frac{e^{-2.5r}}{2.5r}\right] \text{MeV} \\ v_{01}(r) &= \left[-4885.5\frac{e^{-4r}}{4r} + 1175.5\frac{e^{-2.5r}}{2.5r}\right] \text{MeV}. \end{aligned} \tag{2.117}$$

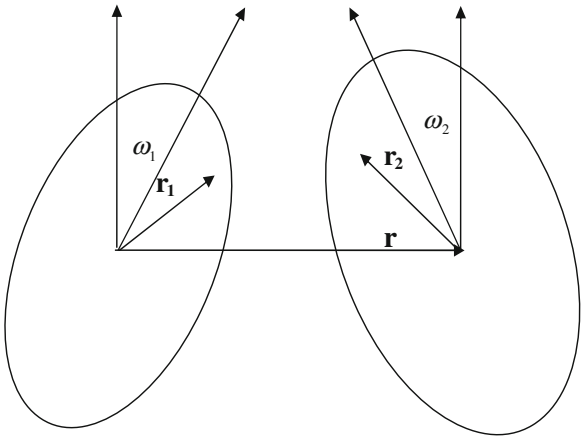

Fig. 2.13 Geometry of the double folding interaction

The second term in Eq. 2.116 approximates the single-nucleon exchange effects through a zero-range pseudopotential with the strength $\hat{J}_{00} = -262\,\text{MeV fm}^3$.

Let us consider for simplicity that both nuclei are axially symmetric, but the generalization to the triaxial case is straightforward. The radial components of the nuclear densities are given by the standard multipole expansion, which can be written in both intrinsic and laboratory systems of coordinates as follows

$$\begin{aligned}\rho(\alpha_k, \mathbf{r_k}) &= \sum_{\lambda} \rho_{\lambda}(\alpha_k, r_k) Y_{\lambda 0}(\hat{r}'_k) \\ &= \sum_{\lambda\mu} \rho_{\lambda}(\alpha_k, r_k) D^{\lambda}_{\mu 0}(\omega_k) Y_{\lambda\mu}(\hat{r}_k), \quad k = 1, 2.\end{aligned} \tag{2.118}$$

We then expand the two-body interaction in Fourier components

$$v(\mathbf{r} + \mathbf{r}_2 - \mathbf{r}_1) = \int q^2 dq d\hat{q} \tilde{v}(q) e^{i\mathbf{qr}} e^{i\mathbf{qr}_2} e^{-i\mathbf{qr}_1}, \tag{2.119}$$

where one has for the Yukawa-like interaction

$$\tilde{v}(q) = \frac{1}{(2\pi)^3} \int v_0 \frac{e^{ikr}}{r} e^{i\mathbf{q}.\mathbf{r}} d\mathbf{r} = \frac{1}{(2\pi)^3} \frac{4\pi v_0}{q^2 + k^2}. \tag{2.120}$$

By using the multipole representation of the plane wave

$$e^{i\mathbf{q}.\mathbf{r}} = 4\pi \sum_{l} i^l j_l(qr) \sum_{m} Y_{lm}(\hat{q}) Y^*_{lm}(\hat{r}), \tag{2.121}$$

we obtain

$$V(\alpha_1, \alpha_2, \omega_1, \omega_2, \mathbf{r}) = V_0(\alpha_1, \alpha_2, r) + V_d(\alpha_1, \alpha_2, \omega_1, \omega_2, \mathbf{r}), \tag{2.122}$$

where the deformed part of the potential is given by

$$V_d(\alpha_1,\alpha_2,\omega_1,\omega_2,\mathbf{r}) = \sum_{\lambda_1\lambda_2\lambda_3} V_{\lambda_1\lambda_2\lambda_3}(\alpha_1,\alpha_2,r) \times \left\{ \left[D_0^{\lambda_1}(\omega_1) \otimes D_0^{\lambda_2}(\omega_2) \right]_{\lambda_3} \otimes Y_{\lambda_3}(\hat{r}) \right\}_0 . \tag{2.123}$$

Here the term $(\lambda_1\lambda_2\lambda_3) = (000)$ is excluded from summation. The radial formfactor in (2.123) is given by the integration over the angular coordinate $\hat{q}$

$$V_{\lambda_1\lambda_2\lambda_3}(\alpha_1,\alpha_2,r) = i^{\lambda_1-\lambda_2+\lambda_3}\frac{(4\pi)^3}{\sqrt{4\pi}}\hat{\lambda}_1\hat{\lambda}_2\langle\lambda_1,0;\lambda_2,0|\lambda_3,0\rangle \times \int_0^\infty q^2 dq\tilde{v}(q)\tilde{\rho}_{\lambda_1}(q)\tilde{\rho}_{\lambda_2}(q)j_{\lambda_3}(qr). \tag{2.124}$$

where we introduced the radial Fourier transform of densities

$$\tilde{\rho}_{\lambda_k}(q) = \int_0^\infty r_k^2 dr_k \rho_{\lambda_k}(r_k) j_{\lambda_k}(qr_k). \tag{2.125}$$

The spherical part of the potential can be written as a particular case of the above double folding potential, i.e.

$$V_0(\alpha_1,\alpha_2,r) = \frac{1}{\sqrt{4\pi}} V_{000}(\alpha_1,\alpha_2,r). \tag{2.126}$$

In the following we will describe various particular cases of the inter-fragment potential.

2.9.1 Boson Emission

Let us consider that both fragments are even–even nuclei with internal structure, like for instance in fission processes. They are left in ground or excited state and this kind of spectroscopy is characterized by a double fine structure.

Experimental measurements by electron scattering and microscopic calculations showed that the density distribution of fragments can be approximated by a Fermi-like shape, i.e.

$$\rho(\alpha_k,\mathbf{r}'_k) = \frac{\rho_k^{(0)}}{1+e^{[r_k-R(\hat{r}'_k)]/a_k}}, \quad k=1,2, \tag{2.127}$$

where the radius of the nuclear surface is given by

$$R(\hat{r}'_k) = R_0\left[1+\sum_{\lambda>0}\sum_{v}\alpha_{\lambda v}Y_{\lambda v}(\hat{r}'_k)\right], \tag{2.128}$$

and the central densities are normalized by the total number of protons and neutrons separately.

The case when $\lambda_2 = 0$, $\lambda_1 = \lambda_3 = \lambda$ describes the emission of a structureless particle "2" in the field of the daughter nucleus "1". This kind of spectroscopy is characterized by a single fine structure. The typical case is the α-decay, but the emission of spherical heavy clusters is also described by this particular ansatz. In all these cases the proton density of the light cluster is given by a Gaussian-like distribution, i.e.

$$\rho(\mathbf{r}_2) = \frac{Z_2}{b^3\pi^{3/2}} e^{-(r_2/b)^2}, \tag{2.129}$$

and a similar expression for the neutron density. The parameter of the distribution width is $b = 1.19$ fm for an α-particle, $b = 1.58$ fm for ^{12}C, $b = 1.74$ fm for ^{14}C [36]. The expansion (2.123) becomes the usual multipole–multipole interaction

$$V(\alpha, \omega, \mathbf{r}) = V_0(\alpha, r) + \sum_{\lambda > 0} V_\lambda(\alpha, r) \sum_\mu D^\lambda_{\mu 0}(\omega) Y_{\lambda\mu}(\hat{r}). \tag{2.130}$$

The last sum over μ represents nothing else but the rotation (by Euler angles ω) in the intrinsic system of coordinates

$$V(\alpha, \mathbf{r}') = V_0(\alpha, r) + \sum_{\lambda > 0} V_\lambda(\alpha, r) Y_{\lambda 0}(\hat{r}'). \tag{2.131}$$

2.9.2 Fermion Emission

Let us suppose that the light particle is a fermion (proton or neutron) and the daughter nucleus has axial symmetry. The interaction potential is given by the following ansatz

$$V(\mathbf{x}, \mathbf{r}, \mathbf{s}) = V_0(r, \mathbf{s}) + V_d(\mathbf{x}, \mathbf{r}, \mathbf{s}), \tag{2.132}$$

where $V_0(r, \mathbf{s})$ is the spherical component of the interaction

$$V_0(r, \mathbf{s}) \equiv V_0(r) + V_{\rm so}(r)\mathbf{l}\cdot\boldsymbol{\sigma}. \tag{2.133}$$

Here $V_0(r)$ is the central interaction between the left nucleus and the fermion, while $V_{\rm so}(r)$ is the spin-orbit interaction ($\sigma = 2s$). The central potential includes the nuclear part $V_N(r)$ and the Coulomb interaction $V_C(r)$. The folding procedure gives as a result the nuclear potential with a Woods–Saxon shape, like it is given in Fig. 2.1.

The deformed part can be written in a similar way as (2.130), i.e.

$$V_d(\mathbf{x},\mathbf{r},\mathbf{s}) \equiv \sum_{\lambda>0} V_\lambda(r,\mathbf{s}) Q_\lambda(\mathbf{x}) \cdot T_\lambda(\hat{r}). \tag{2.134}$$

The scalar product is, as usually, $Q_\lambda(\mathbf{x}) \cdot T_\lambda(\hat{r}) = \sum_\mu Q^*_{\lambda\mu}(\mathbf{x}) T_{\lambda\mu}(\hat{r})$where$Q_{\lambda\mu}(\mathbf{x})$ is the λ-pole operator which depends upon the collective coordinate $\mathbf{x}$. For example, in the case of collective rotations this coordinate corresponds to the Euler rotation angles $\omega \equiv (\phi, \theta, \psi)$, while for vibrational modes it corresponds to the quadrupole coordinates $\alpha_{2\mu}$.

The multipole operator $T_{\lambda\mu}$ has a more complex structure, as it is given in Appendix (14.1), i.e.

$$\begin{aligned} V_\lambda(r,\mathbf{s}) Q_\lambda(\mathbf{x}) \cdot T_\lambda(\hat{r}) &\to V_{c,\lambda}(r) Q_\lambda(\mathbf{x}) \cdot Y_\lambda(\hat{r}) \\ &+ V^{(\lambda-1)}_{\mathrm{so},\lambda}(r) Q_\lambda(\mathbf{x}) \cdot T^{(\lambda-1)}_\lambda(\hat{r},\sigma) + V^{(\lambda+1)}_{\mathrm{so},\lambda}(r) Q_\lambda(\mathbf{x}) \cdot T^{(\lambda+1)}_\lambda(\hat{r},\sigma), \end{aligned} \tag{2.135}$$

where the differential operator $T^{(\lambda\pm1)}_{\lambda\mu}$ is defined in Eq. 14.33 and describes the deformed spin-orbit part of the mean field.

2.9.3 Vibrational Nuclei

Let us consider an emission process where the light particle is structureless (a proton or an α-particle) and the heavy fragment is left in a vibrational state. Let us also suppose that the deformed interaction (2.131) has equipotential surfaces given by the ansatz (2.128). This means that the potential an be written as follows

$$V(\alpha,\mathbf{r}') = V\left(\frac{r}{1+\sum_{\lambda>0}\sum_\nu \alpha_{\lambda\nu} Y_{\lambda\nu}(\hat{r}')}\right). \tag{2.136}$$

By expanding this function around the spherical shape one obtains the general form of the interaction between a vibrational core and the emitted light particle

$$\begin{aligned} V(\alpha,\mathbf{r}') &\approx V(0,r) + \sum_{\lambda>0}\sum_\nu \frac{\partial V(0,r)}{\partial \alpha_{\lambda\nu}} \alpha_{\lambda\nu} \\ &= V(0,r) - r\frac{\partial V(0,r)}{\partial r} \sum_{\lambda>0}\sum_\nu \alpha_{\lambda\nu} Y_{\lambda\nu}(\hat{r}'). \end{aligned} \tag{2.137}$$

In the laboratory system it becomes

$$V(\alpha,\omega,\mathbf{r}') = V_0(0,r) - r\frac{\partial V_\lambda(0,r)}{\partial r} \sum_{\lambda>0}\sum_{\mu\nu} \alpha_{\lambda\nu} D^\lambda_{\mu\nu}(\omega) Y_{\lambda\mu}(\hat{r}). \tag{2.138}$$

2.9.4 Triaxial Nuclei

The above potential is a particular case of a general triaxial interaction

$$\begin{aligned} V(\omega,\mathbf{r},\mathbf{s}) &= V_0(r,\mathbf{s}) + \sum_{\lambda>0} V_\lambda(r,\mathbf{s})\cdot D^\lambda(\omega)\cdot T_\lambda(\hat{r}), \\ &\equiv V_0(r,\mathbf{s}) + \sum_{\lambda>0,\mu} V_{\lambda\mu}(r,\mathbf{s}) \sum_\nu D^\lambda_{\nu\mu}(\omega) T_{\lambda\nu}(\hat{r}), \end{aligned} \tag{2.139}$$

where the multipole operators $T_{\lambda\mu}$ correspond to the usual spherical harmonics for the central part of the potential, while for the spin-orbit interaction (which includes derivatives) $T_{\lambda\mu}$ are the differential operators given by Eq. 14.33.

Therefore, one obtains in the intrinsic system the expression

$$V(\omega,\mathbf{r}',\mathbf{s}) = V_0(r,\mathbf{s}) + \sum_{\lambda>0,\mu} V_{\lambda\mu}(r,\mathbf{s}) T_{\lambda\mu}(\hat{r}'). \tag{2.140}$$

2.10 Spectroscopic Factor

The above described double folding procedure supposes that the two fragments are already born. The parameters of the M3Y interaction (2.117) correspond to a double folding potential describing the heavy ion scattering. Yet, the wave function describing the emission process $P \to D + C$, where $P(D)$ is the parent (daughter) nucleus, has a cluster-like ansatz, i.e. it is a superposition of different mutually orthogonal channel components, similar with Eq. 2.59

$$\Psi_{J_iM_i}(\mathbf{x}_P,\mathbf{r}) \to \sum_c \mathscr{F}_c(r)\mathscr{Y}^{(c)}_{J_iM_i}(\mathbf{x}_D,\mathbf{x}_C,\hat{r}), \tag{2.141}$$

where $\mathbf{x}$ indicates the internal coordinate. We did not write the equality sign because, in general, the wave function of the initial configuration, given by the left hand side, does not contain a 100% cluster-like representation, as it is written by the right hand side.

Indeed, the ratio between the computed half life, by using the phenomenological double folding potential, and the experimental value is less than unity. It is called phenomenological spectroscopic factor

$$S = \frac{T_{\text{phen}}}{T_{\text{exp}}}. \tag{2.142}$$

This is due to the fact that actually the emitted fragments do not exist during the decay process, but they are born with certain probability. In deriving the expression of the decay width (2.83) we divided the outgoing flux to the volume integral of the wave function squared over the internal volume, by considering its value

unity. Actually this volume integral gives the creation probability of emitted fragments.

The amplitude of the cluster-like ansatz contained in the initial wave function (2.141) is the overlap between the initial wave function and the product between the internal wave functions of the emitted fragments

$$\mathscr{F}_c(r) = \langle \mathscr{Y}^{(c)}_{J_i M_i} | \Psi_{J_i M_i} \rangle. \tag{2.143}$$

It is also called preformation amplitude and will be extensively analyzed in the second part of the book. Here, we only give the main ideas connected with this concept.

2.10.1 Particle Emission

For a proton emission from an odd–even emitter, connecting deformed nuclei in their ground states, the channel is given by the spin projection, i.e. $c \equiv K$. Let us denote by $a^{\dagger}_{\pi K}$ the *particle* creation operator ($\pi =$ proton). The initial wave function in the pairing approach is a superposition of different proton excitations of the parent Bardeen–Cooper–Schriffer (BCS) vacuum $\alpha^{\dagger}_{\pi K}|\mathrm{BCS}_{\pi P}\rangle$. Since

$$a^{\dagger}_{\pi K}|\mathrm{BCS}_{\pi D}\rangle = \left[u^{(D)}_{\pi K}\alpha^{\dagger}_{\pi K} + v^{(D)}_{\pi K}\alpha_{\pi \overline{K}}\right]|\mathrm{BCS}_{\pi D}\rangle. \tag{2.144}$$

The preformation amplitude becomes

$$\mathscr{F}_K \equiv \langle \mathrm{BCS}_{\pi D}|a_{\pi K}\alpha^{\dagger}_{\pi K}|\mathrm{BCS}_{\pi P}\rangle = u^{(D)}_{\pi K}\langle \mathrm{BCS}_{\pi D}|\mathrm{BCS}_{\pi P}\rangle \approx u^{(D)}_{\pi K}. \tag{2.145}$$

where the last approximation reflects the blocking effect of the odd proton. It is important to point out that in proton emission the spectroscopic amplitude $\mathscr{F}_K$ is a constant, corresponding to the BCS amplitude around the Fermi surface, i.e. $u_K \sim \sqrt{0.5}$. It multiplies the scattering amplitude N_K.

2.10.2 Cluster Emission

The situation changes for cluster emission. The preformation amplitude (2.143) is a function of the radius between emitted fragments and it plays the role of the "internal" wave function. It should satisfy the matching condition with respect to the corresponding "external" channel radial component at certain radius R, i.e.

$$\begin{aligned}\mathscr{F}_c(R) &= \frac{f_c(R)}{R} \\ \mathscr{F}'_c(R) &= \left[\frac{f_c(r)}{r}\right]'_{r=R}.\end{aligned} \tag{2.146}$$

In the second part, devoted to microscopic approaches, we will analyze in detail the properties of the preformation amplitude. Here we give only some preliminary details.

Let us illustrate how to estimate the overlap integral (2.143) in the case of α-decays involving transitions between ground states. The main idea is to find an α-like four body creation operator connecting daughter with parent nuclei, i.e.

$$|\Psi_P\rangle = P_\alpha^\dagger |\Psi_D\rangle. \tag{2.147}$$

If both parent and daughter are deformed nuclei, described within the pairing approach, than one has the following factorization

$$P_\alpha^\dagger = P_\pi^\dagger P_\nu^\dagger, \tag{2.148}$$

in terms of proton and neutron two body creation operators

$$P_\tau^\dagger = \sum_{K>0} X_{\tau K} a_{\tau K}^\dagger a_{\tau \overline{K}}^\dagger, \ \tau = \pi, \nu. \tag{2.149}$$

The expansion coefficients are given by the following ansatz

$$X_{\tau K} = \langle \mathrm{BCS}_{\tau P} | a_{\tau K}^\dagger a_{\tau \overline{K}}^\dagger | \mathrm{BCS}_{\tau D} \rangle \approx u_{\tau K}^{(D)} v_{\tau K}^{(D)}. \tag{2.150}$$

Thus the overlap integral becomes

$$\mathscr{F}_\alpha(\mathbf{r}) = \langle \Psi_D \Psi_\alpha | P_\alpha^\dagger | \Psi_D \rangle = \sum_{KK'>0} X_{\pi K} X_{\nu K'} \langle \Psi_\alpha | a_{\pi K}^\dagger a_{\pi \overline{K}}^\dagger a_{\nu K'}^\dagger a_{\nu \overline{K}'}^\dagger | 0 \rangle, \tag{2.151}$$

where Ψ_α is the α-particle wave function, written as a product of three Gaussians in relative proton–neutron coordinates [37–39]. This four-body overlap integral will be computed in the second part of the book, by using the standard recoupling of two proton and two neutron single particle states, from absolute to the relative and center of mass coordinates [40].

In the case of the cluster emission, one obtains a similar representation [41]. For instance in ^{14}C emission a good approximation of the parent wave function, at distances where Pauli principle is less important, is given by

$$|\Psi_P\rangle \approx P_{\alpha_1}^\dagger P_{\alpha_2}^\dagger P_{\alpha_3}^\dagger P_\nu^\dagger |\Psi_D\rangle, \tag{2.152}$$

and the preformation factor is given by a similar expression, i.e.

$$\mathscr{F}_{^{14}\mathrm{C}}(\mathbf{r}) = \langle \Psi_D \Psi_{^{14}\mathrm{C}} | P^{\dagger}_{\alpha_1} P^{\dagger}_{\alpha_2} P^{\dagger}_{\alpha_3} P^{\dagger}_{\nu} | \Psi_D \rangle, \tag{2.153}$$

where $\Psi_{^{14}\mathrm{C}}$ is the ^{14}C wave function, written as a product of several Gaussians in relative coordinates.

One defines the microscopic spectroscopic factor for transitions connecting ground states by the following integral

$$S_{\mathrm{gs}} = \sum_c \int_0^{\infty} |r\mathscr{F}_c(r)|^2 dr. \tag{2.154}$$

It gives the order of magnitude of the cluster content inside the parent wave function. In principle it should have the same order of magnitude as the spectroscopic factor defined by Eq. 2.142. Actually they are quite different and the ratio S/S_{gs} defines the amount of the additional clustering with respect to the microscopic estimate, given by the preformation amplitude (2.143).

References

1. Unger, H.-J.: On the factorisation of the wave function and the green function in the region of isolated poles of the S-function. Nucl. Phys. A **104**, 564–576 (1967)
2. Gamow, G.: Zur Quantentheorie des Atomkernes. Z. Phys. **51**, 204–212 (1928)
3. Condon, E.U., Gurwey, R.W.: Wave mechanics and radioactive disintegration. Nature **22**, 439 (1928)
4. Civitarese, O., Gadella, M.: Physical and mathematical aspects of Gamow States. Phys. Rep. **396**, 41–113 (2004)
5. Abramowitz, M., Stegun, I.A. (eds.): Handbook of Mathematical Functions. Dover Publications Inc., New York (1983)
6. Lane, A.M., Thomas, R.G.: R-Matrix theory of nuclear reactions. Rev. Mod. Phys. **30**, 257–353 (1958)
7. Vertse, T., Liotta, R.J., Maglione, E.: Exact and approximate calculation of giant resonances. Nucl. Phys. A **584**, 13–34 (1995)
8. Berggren,T.: The use of resonant states in Eigenfunction expansions of scattering and reaction amplitudes. Nucl. Phys. A **109**, 265–287 (1968)
9. Berggren, T.: On the interpretation of cross sections for production of resonant final states. Phys. Lett. B **73**, 389–392 (1978)
10. Breit, G., Wigner, E.P.: Capture of slow neutrons. Phys. Rev. **49**, 519–531 (1936)
11. Teichmann, T., Wigner, E.P.: Sum rules in the dispersion theory of nuclear reactions. Phys. Rev. **87**, 123–135 (1952)
12. Thomas, R.G.: A formulation of the theory of alpha-particle decay from time-independent equations. Prog. Theor. Phys. **12**, 253–264 (1954)
13. Ixaru, L., Rizea, M., Vertse, T.: Piecewiese perturbation methods for calculating Eigensolutions of complex optical potential. Comput. Phys. Commun. **85**, 217–230 (1995)
14. Vertse, T., Pál, K.F., Balogh, A.: GAMOW, a program for calculating the resonant state solution of the Radial Schrödinger Equation in an arbitrary optical potential. Comput. Phys. Commun. **27**, 309–322 (1982)

15. Taylor, J.R.: Scattering Theory. Wiley, New York (1972)
16. Geiger, H., Nuttall, J.M.: The ranges of the α particles from various substances and a relation between range and period of transformation. Philos. Mag. **22**, 613–621 (1911)
17. Geiger, H.: Reichweitemessungen an α-Strahlen. Z. Phys. **8**, 45–57 (1922)
18. Sonzogni, A.A.: Proton radioactivity in $Z > 50$ nuclides. Nucl. Data Sheets **95**, 1–48 (2002)
19. Delion, D.S., Liotta, R.J., Wyss, R.: Theories of proton emission. Phys. Rep. **424**, 113–174 (2006)
20. Delion, D.S., Liotta, R.J., Wyss, R.: Systematics of proton emission. Phys. Rev. Lett. **96**, 072501/1–4 (2006)
21. Goldansky, V.I.: On neutron deficient isotopes of light nuclei and the phenomena of proton and two-proton radioactivity. Nucl. Phys. **19**, 482–495 (1960)
22. Viola, V.E., Seaborg, G.T.: Nuclear systematics of the heavy elements-II. J. Inorg. Nucl. Chem. **28**, 741–761 (1966)
23. Hatsukawa, Y., Nakahara, H., Hoffman, D.C.: Systematics of alpha decay half lives. Phys. Rev. C **42**, 674–682 (1990)
24. Brown, B.A.: Simple relation for alpha decay half-lives. Phys. Rev. C **46**, 811–814 (1992)
25. Denisov, V.Y., Khudenko, A.A.: α-Decay half-lives: empirical relations. Phys. Rev. C **79**, 054614/1–5 (2009)
26. Poenaru, D.N., Nagame, Y., Gherghescu, R.A., Greiner, W.: Systematics of cluster decay modes. Phys. Rev. C **65**, 054308/1–6 (2002)
27. Qi, C., Xu, F.R., Liotta, R.J., Wyss, R.: Universal decay law in charged-particle emission and exotic cluster radioactivity. Phys. Rev. Lett. **103**, 072501/1–4 (2009)
28. Ren, Z., Xu, C., Wang, Z.: New perspective on complex cluster radioactivity of heavy nuclei. Phys. Rev. C **70**, 034304/1–8 (2004)
29. Mirea, M., Delion, D.S., Săndulescu, A.: Microscopic cold fission yields of ^{252}Cf. Phys. Rev. C **81**, 044317/1–4 (2010)
30. Delion, D.S.: Universal decay rule for reduced widths. Phys. Rev. C **80**, 024310/1–7 (2009)
31. Blendowske, R., Fliessbach, T., Walliser, H.: From α-decay to exotic decays—a unified model. Z. Phys. A **339**, 121–128 (1991)
32. Medeiros, E.L., Rodrigues, M.M.N., Duarte, S.B., Tavares, O.A.P.: Systematics of half-lives for proton radioactivity. Eur. J. Phys. A **34**, 417–427 (2007)
33. Lovas, R.G., Liotta, R.J., Insolia, A., Varga, K., Delion, D.S.: Microscopic theory of cluster radioactivity. Phys. Rep. **294**, 265–362 (1998)
34. Carstoiu, F., Lombard, R.J.: A new method of evaluating folding type integrals. Ann. Phys. (NY) **217**, 279–303 (1992)
35. Bertsch, G., Borysowicz, J., McManus, H., Love, W.G.: Interactions for inelastic scattering derived from realistic potentials. Nucl. Phys. A **284**, 399–419 (1977)
36. Dao Khoa, T.: α-Nucleus potential in the double-folding model. Phys. Rev. C **63**, 034007/1–15 (2001)
37. Mang, H.J., Rasmussen, J.O.: Mat. Fys. Skr. Dan. Vid. Selsk. **2**(3), (1962)
38. Mang, H.J.: Alpha decay. Ann. Rev. Nucl. Sci. **14**, 1–28 (1964)
39. Poggenburg, J.K., Mang, H.J., Rasmussen, J.O.: Theoretical alpha-decay rates for the Actinide region. Phys. Rev. **181**, 1697–1719 (1969)
40. Delion, D.S., Insolia, A., Liotta, R.J.: New single particle basis for microscopic description of decay processes. Phys. Rev. C **54**, 292–301 (1996)
41. Delion, D.S., Insolia, A., Liotta, R.J.: Pairing correlations and quadrupole deformation effects on the ^{14}C decay. Phys. Rev. Lett. **78**, 4549–4552 (1997)